

ABSTRACT

Title of thesis: MODELING, ESTIMATION, AND CONTROL
 OF ACTUATOR DYNAMICS FOR REMOTELY
 OPERATED UNDERWATER VEHICLES

Jordan A. Boehm, Master of Science, 2019

Thesis directed by: Professor Derek A. Paley
 Department of Aerospace Engineering
 Institute for Systems Research

Modeling and control of remotely operated underwater vehicles is a challenging problem that depends greatly on how the dynamics of their thrusters are compensated. In this thesis a novel method for characterizing thruster dynamics using a six-axis load cell is presented. Multiple dynamic models are characterized with this test setup. Model-based control design strategies are used to compensate for nonlinearities in the dynamics, which include input dead zones and coupling with fluid dynamics. Multiple estimation methods are presented to construct an estimate of fluid velocity which is handled as an unmeasured state. The different models, controllers, and estimators are comparatively evaluated in closed-loop experiments using the six-axis load cell to measure thrust tracking performance. Full vehicle simulations using the experimentally characterized models provide additional opportunities for comparison of control and estimation strategies. The potential tracking control benefits from the variety of presented thruster dynamics compensation strategies are evaluated for a remotely operated underwater vehicle with multiple thrusters.

MODELING, ESTIMATION, AND CONTROL OF ACTUATOR
DYNAMICS FOR REMOTELY OPERATED UNDERWATER
VEHICLES

by

Jordan A. Boehm

Thesis submitted to the Faculty of the Graduate School of the
University of Maryland, College Park in partial fulfillment
of the requirements for the degree of
Master of Science
2019

Advisory Committee:
Professor Derek A. Paley, Chair/Advisor
Professor David Akin, Co-Advisor
Professor Robert M. Sanner

© Copyright by
Jordan A. Boehm
2019

Dedication

To my parents, who encouraged me to always pursue new experiences and learn from my own mistakes.

“Research is what I’m doing when I don’t know what I’m doing.”

–Wernher von Braun

Acknowledgments

I owe my gratitude to so many people who made this work possible. While I will try my best to include everyone, there will inevitably be those who are inadvertently left out. I apologize if anyone is not mentioned, but know that I value your support greatly. Perhaps the most important person to thank is my advisor, Dr. Derek Paley, for granting me the opportunity to work on this project and providing such insightful guidance and feedback during my time working with him. The amount of personal growth I have achieved through his encouragement and instruction has been so much greater than I could have anticipated. For that I will always be grateful.

I additionally want to thank my committee, Dr. David Akin and Dr. Robert Sanner, for offering their time and expertise to provide meaningful and valuable feedback to my work. My experiences as an undergraduate in Dr. Paley's, Sanner's, and Akin's courses inspired me to pursue this research and the thought-provoking challenges they have provided me in their graduate courses continue to influence how I investigate and approach engineering problems today. I would not have realized my own love for this field if it were not for the profound knowledge I gained under your instruction. Other faculty I owe thanks to are Dr. Raymond Sedwick and Dr. Mumu Xu who guided me through my undergraduate research projects and encouraged me to stay curious and vigilant in my academic endeavors.

I want to give another big thank you to those in the Aerospace Department who helped me in my process through the undergraduate and graduate programs.

Aileen Hentz, Tom Hurst, Otto Fandino, LaVita Williams, Gabrielle Madison, Matt Sinclair, and all my other friends in the department have been great sources of assistance during my time here. I owe special gratitude to Aileen Hentz and Tom Hurst, who offered their time and guidance during my transition from the undergraduate program. When I was uncertain of my post-graduation path, you provided such kind and constructive guidance that led me to where I am today. I cannot be more thankful for that.

To my friends and colleagues at National Geographic, thank you for being such fantastic team members. Thank you Eric Berkenpas, Mike Shepard, Kyler Abernathy, Brad Henning, Alan Turchik, Arthur Clarke, Mohsen Samak, Cody Goldhahn, Michelle Rodriguez, and Jessica Elfadl for being great friends and providing amusingly witty conversations during countless hours working on this project. I especially am thankful to Eric Berkenpas and Mike Shepard for their valuable guidance and assistance in this project while always remaining upbeat and amusing. I have really come out of my shell during these past two years thanks to all of you.

I would be remiss not to acknowledge my CDCL family who I have come to know so well in graduate school more so than any other group. Thank you to Travis Burch, Daniel Gomez, Brian Free, Will Craig, Will Scott, Artur Wolek, Debdipta Goswami, Jinseong Lee, Helene Nguewou, Sheng Cheng, Paul Ghanem, as well as all undergraduates including Jimmy Witkoski who had a part in this work. I owe special thanks to Travis Burch and Daniel Gomez for being great friends and colleagues during countless homeworks, projects, and editing sessions. Thank you also to Girguis Sedky, Jamie King, Kate Melone, Jackson Shannon, Eric Frizzell,

Mark Moretto, Dominick Montero, Priya Dharmavaram, Angelina Nou, Katherine Smolen, and so many other classmates who offered conversation and companionship over the years.

Thank you to my family for being so supportive and patient (when necessary) with me during any and all difficult patches that have been a part of my journey through college. You have had 24 years to get good at it, but I know I still find ways to make offering your help and advice difficult. Thank you, regardless of my behavior, for listening to my issues and rantings, and for still being able to provide support and advice when you could. Thank you, Mom and Dad, for encouraging me to pursue precisely what I want in life, and nothing less. Thank you also for showing me how success can be its own reward, and how mistakes are always learning experiences. The freedom you gave me during my childhood played a huge part in how I have grown into the person I am today, and I always value having been able to learn my values through my own experiences rather than by excessive guidance. Thank you also to my aunts Leah, Jo Anne, and Soupy for being so supportive of my hobbies and musical endeavors, and offering wonderful conversation on those topics. Thank you to my Grandfather for being a constant source of guidance and wisdom in my life, and inspiring me to pursue bold endeavors, and to my Grandmother who did not get to see me grow up and achieve what I have, but who I know is proud of me.

Thank you to my friends who have been great sources of joy and support over the years. Thank you Matt and Brett for being the two best friends I could have ever asked for, and for remaining great sources of support, jokes, and activities all

these years and for years to come. Thank you to Emily for always believing in me and supporting me even when we have disagreements. You have been a vital companion in my life for years now and I hope will remain so for countless years to come. Thank you also to the Bertots for being a second family to me over these years. Thank you to my college family: Nick, Jacob, Matt, Steve R., Steve B., Nate, and Steph for being fantastic friends.

Thank you also to past friends and teachers who may not have been mentioned here. To Lynda Motiram, Kai Frick, Ruth Goldstraw, Ellen Lehrter, Laura Volkov, Lindsay Reed, Erin Few, Mike Miller, Andrea Linnell, and Lynn Clough for being important influences in my education. You made such an important impact on my life for encouraging me to pursue my interests that I will always be grateful for.

Thank you to Elana and Xiaofang for your helpful feedback and guidance through these past few years. Thank you to Donald Fagen for being a constant source of inspiration in my life, as well as his colleague Walter Becker whose untimely passing occurred while this work was being completed. Thank you additionally to all the sources of discouragement I have met in my life for serving to strengthen my resolve and conviction. Perhaps Juan Goytisolo said it best: “To those who inspired it and will not read it.” Thank you to all those I have not mentioned but have impacted me in one way or another.

Finally, this research would not have been possible without the support of the National Geographic graduate research fellowship that funded it. I gratefully acknowledge that support.

Table of Contents

Dedication	ii
Acknowledgements	iii
List of Tables	ix
List of Figures	x
1 Introduction	1
1.1 Motivation	1
1.2 Relation to State of the Art	2
1.3 Technical Approach	4
1.4 Contributions of Thesis	6
1.5 Outline of Thesis	8
2 Background: Underwater Vehicle Modeling and Control	9
2.1 Underwater Vehicle Dynamics	9
2.2 Underwater Vehicle Control	16
3 Simplified Thruster Modeling and Control	18
3.1 Experimental Characterization of Model Parameters	18
3.1.1 Experimental Setup	18
3.1.2 Experimental Procedure	22
3.2 Simplified Thruster Model	23
3.3 Feedback Control Strategy	29
3.3.1 Single-Thruster Control	29
3.3.2 Full Vehicle Control	33
4 Hydrodynamic Thruster Modeling and Control	36
4.1 Experimental Characterization of Model Parameters	37
4.1.1 Experimental Setup	37
4.1.2 Experimental Procedure	38
4.2 Hydrodynamic Thruster Model	39

4.3	State Estimation Methods	46
4.4	Feedback Control Strategy	48
5	Performance Evaluation of Thrust Control	51
5.1	Experimental Performance of Single-Thruster Control	52
5.1.1	Experimental Methodology	52
5.1.2	Discussion of Results	54
5.2	Simulated Performance of Full Vehicle Control	58
5.2.1	Simulations with Simple Thruster Model	59
5.2.2	Simulations with Hydrodynamic Thruster Model	61
6	Conclusion	67
6.1	Summary of Contributions	67
6.2	Suggestions for Ongoing and Future Work	69
	Bibliography	71

List of Tables

3.1	Simplified Model Parameter Values	28
4.1	Hydrodynamic Model Parameter Values	45
4.2	HL & HQ Paramater Values	45

List of Figures

1.1	Computer rendering of the ROV under development by the National Geographic Society.	5
1.2	Images of Tecnydyne thruster used for testing and modeling in this work.	6
3.1	Load cell used in model characterization.	19
3.2	Diagram of load cell with principal axes and attachment points marked.	20
3.3	Block diagram of experimental data collection system.	23
3.4	Steady-state thrust and torque models compared to experimental data.	24
3.5	Step responses of thrust, torque, and rotor speed models compared to experimental data.	25
3.6	Steady-state propeller angular velocity data.	27
3.7	Control simulations driving a thruster to a setpoint n_d with consideration for \dot{u}_{max}	33
4.1	Annotated image of experimental setup with load cell and ADV used in model characterization.	38
4.2	Model fit results from system identification procedures done for hydrodynamic thruster models. Fits shown for (a) angular velocity, (b) fluid velocity, (c) thrust, and (d) torque.	40
4.3	Diagram of how physically relevant values in thruster models relate to the thruster system.	42
5.1	Block diagram of the feedback loop used for experimental output feedback tests of the thruster. When using the simplified model for control purposes, inclusion of v and U is omitted from this framework.	53
5.2	Tracking performance of thrust for the step experimental run.	55
5.3	Tracking performance of thrust for the triangle wave experimental run.	55
5.4	Tracking performance of thrust for the sine wave experimental run.	56
5.5	Thrust Tracking RMSE normalized by the RMSE of the lookup table method for all control strategies in the test cases for (a) a step, (b) a triangle wave, and (c) a sine wave.	57

5.6	Tracking and estimation performance of angular velocity for the sine wave experimental run.	58
5.7	Estimation performance of axial and ambient velocity for the sine wave experimental run.	59
5.8	Block diagram of the feedback loop used for simulated output feedback tests of the ROV. When using the simplified model for control purposes, inclusion of v is omitted from this framework.	60
5.9	Setpoint tracking performance comparison between the proposed dead-zone-compensating controller and lookup-table-based control for (a) linear forward velocity, (b) angular pitch velocity, and (c) pitch angle.	61
5.10	Tracking errors for each degree of freedom involved in setpoint tracking.	62
5.11	Setpoint tracking performance comparison between all the proposed control strategies for (a) linear forward velocity, (b) angular pitch velocity, and (c) pitch angle.	63
5.12	Tracking errors for each degree of freedom involved in setpoint tracking.	64
5.13	Estimation errors of v for an individual thruster in the previous simulations.	65
5.14	Normalized estimation RMSE of v for each estimator run in simulation.	66

Chapter 1: Introduction

1.1 Motivation

Remotely operated vehicles (ROVs) are widespread and versatile, being applicable to deep-sea exploration and mining [1], marine research [2], hull inspection [3], and wreckage surveying [4]. To accomplish these tasks, ROV control is typically accomplished through a variety of methods ranging from direct human-in-the-loop control to autonomous, logic-driven control [5]. Controllers for autonomous or semi-autonomous operation have been designed through a variety of feedback frameworks, including feedback linearization [6, 7], robust control [8, 9], and adaptive control [9, 10].

Most ROV operations are accomplished by semi-autonomous or full human control, whereby direct commands from an operator are either processed by a controller or fed directly to individual thrusters [5]. Direct-controlled ROVs typically have orthogonal thruster configurations that allow for intuitive translations from commands to thrusts, but such actuator placement can complicate the vehicle design. As a result, fewer thrusters are often used, thus limiting maneuverability of the ROV [5]. To maintain generality, this work analyzes an ROV that has a specific thruster placement configuration to accomplish fully actuated control. An

auto-stabilizing control system is assumed to process user commands into setpoints.

To improve tracking performance of user-defined trajectories, actuator dynamics are often important factors to take into account for controller design [11–13]. This often involves creating a feedback loop on the thrust output of ROV thrusters, which is not a directly measurable quantity in practice [14]. Instead, motor dynamics of thrusters are typically modeled by measurable states like propeller speed which typically can be measured [15]. This means a mathematical model of thrust must be used based on thruster states to determine what commands must be given to achieve a desired thrust. A variety of thrust models have been proposed and remain a common point of research for accurately describing thruster behavior [11, 12, 16].

1.2 Relation to State of the Art

To enhance controller performance and reduce limit-cycle behavior for ROVs, actuator dynamics are typically accounted for in the control design [8, 11, 13, 15, 17–19]. A variety of methods for modeling thrusters for underwater vehicles have been developed in previous work. A two-state axial flow dynamic model [11, 12, 18] accounts for thrust overshoot but is limited to uni-directional flow characterization. A two-state rotational flow model [13] has no more model accuracy than the axial flow model. Lastly, a multi-directional axial flow model [20] requires a large number of parameters to be identified with extensive system testing. This work initially expands upon a single-state voltage-driven thruster model presented in [8]. The system analyzed in this thesis uses an analog voltage signal (throttle) as the control

input for the thruster dynamics, which also exhibit a dead zone nonlinearity. After the single-state dynamics are analyzed, the control results are extended to a higher-order system that accounts for axial fluid velocity.

In previous work, robust and adaptive control techniques have been used for dead zone compensation in the absence of well-identified model parameters [21, 22]. This work utilizes feedback linearization to compensate for nonlinearities in thruster dynamics, because high-quality propeller speed, thrust, and torque data obtained from a six-axis Gough-Stewart platform load cell are available [23].

When extended to higher-order models, thruster dynamics become more difficult to model and compensate in controller designs [8, 18, 20, 24]. Thrust losses due to fluid velocity typically can be well modeled but must be estimated without measurements in practical settings [12, 14, 16, 18]. This complication typically prohibits backstepping designs that could be used for simpler single-state models, and estimation methods also can present issues [25]. An extended Kalman filter (EKF) could be easily implemented on the nonlinear system, but with limited measurements and a highly nonlinear model this risks having the filter diverge [26, 27]. This work opts for a nonlinear observer form for estimating axial velocity in hydrodynamic thruster models that has global convergence guarantees in order to avoid issues presented by the EKF [18, 28].

To identify models for thrusters, often single-axis Bollard pull load cell systems are used to measure thrust [11, 17, 29, 30]. Such loading systems can be prone to error and do not offer characterization of other loads like reaction torque, which may be characterizing in multi-axis loading setups [13, 23]. This work uses a six-axis load

cell oriented in a Gough-Stewart platform design to measure force and moment loads in multiple directions, which allows versatility in characterization capability [31–34]. Gough-Stewart platform-based load cell designs are well documented and analyzed systems, and offer capability to resolve forces and moments along principal axes with great accuracy compared to Bollard systems [31].

1.3 Technical Approach

This work is presented with relevance to the application of ROVs to aquatic imaging, the primary function of an ROV under development by the National Geographic Society (NGS) shown in Fig. 1.1. Underwater filmmaking requires smooth setpoint tracking with human-in-the-loop operations. Reference setpoint attitudes and velocities are typically generated through user input and, for complicated thruster configurations, controllers are capable of effectively tracking commanded trajectories. This is the framework assumed when addressing control problems in this work. Often ROVs maintain only active closed-loop control of three or four degrees of freedom (DOFs), while allowing roll and pitch parameters to be passively stabilized by relying on the natural stability of the vehicle due to the relative locations of the centers of gravity and buoyancy [5,7,8,35,36]. However, for the purposes of deep-sea imaging, it is useful to have full user control of all attitude parameters, similar to a multi-rotor aerial drone, in order to obtain the desired cinematic effects.

Thruster dynamics are compensated by model-based nonlinear control strategies in this work. This is typically done using at least the propeller angular velocity

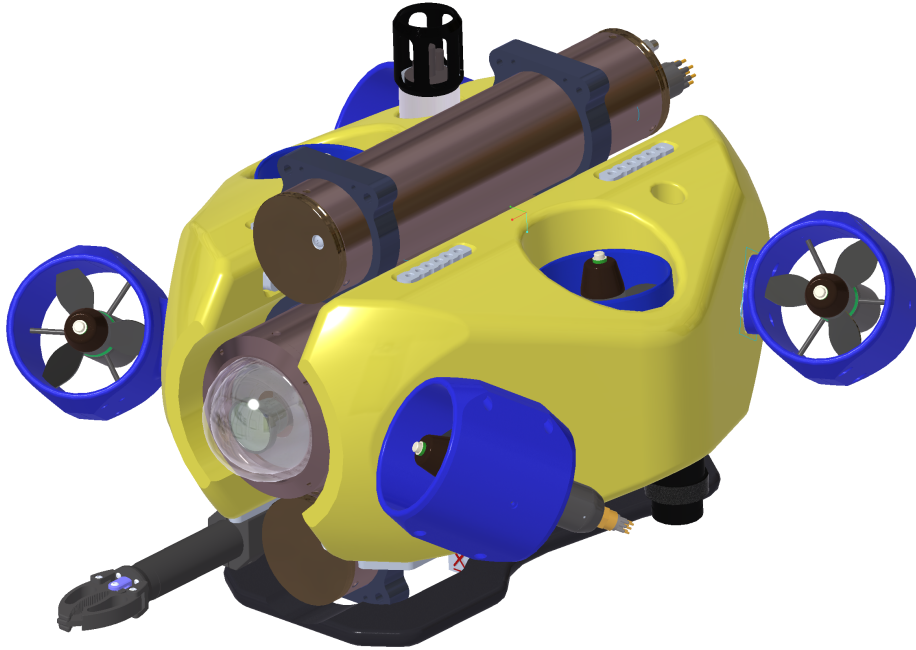


Figure 1.1: Computer rendering of the ROV under development by the National Geographic Society.

as a state, if not with axial fluid velocity through the thruster as another state. The angular velocity is typically measurable via tachometers common in thruster motors, and is also the only directly actuated state. Fluid velocity, in contrast, is not typically directly measurable outside of experimental settings, and is typically only indirectly actuated via the thrust output of the thruster. Due to these factors, estimation methods are necessary to construct an estimate of velocity without direct measurements of the state for the purposes of compensation of fluid velocity effects on thrust [14, 18, 37].

Modeling thruster dynamics and thrust output was completed with a six-axis load cell setup in a Gough-Stewart platform orientation [23]. Fluid velocity measurements for hydrodynamic characterization were obtained with an acoustic

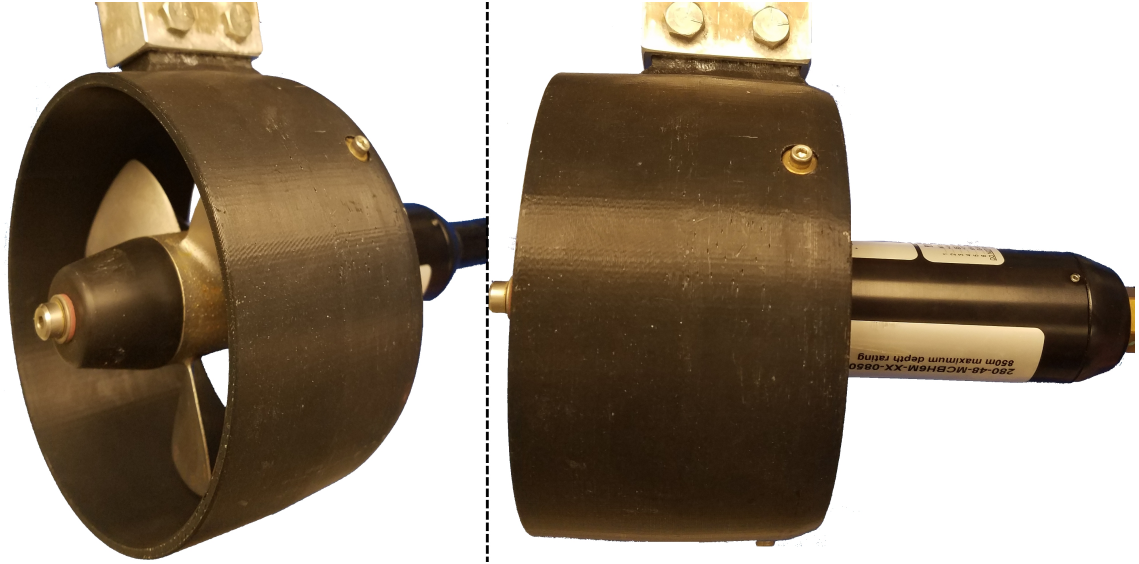


Figure 1.2: Images of Tecnydyne thruster used for testing and modeling in this work.

Doppler velocimeter (ADV). Both the load cell and ADV were utilized in control experiments to have access to ambient fluid velocity measurements for estimation as well as thrust measurements for performance evaluation. A Tecnydyne model 280 thruster was used for all characterization and control experiments (see Fig. 1.2).

1.4 Contributions of Thesis

The contributions of this thesis are:

1. A framework for system identification of multiple dynamic thruster models using a six-axis load cell in a Gough-Stewart platform arrangement. Data processing methods for the load cell are outlined and models are fit using optimization techniques. Extensions to the characterization of thrust losses due to fluid velocity is done with acoustic Doppler velocimeter measurements in tandem with load cell measurements.

2. A nonlinear control law for throttle-controlled thruster dynamics with input dead zones using experimentally obtained parameters. Lyapunov analysis is used to prove stability of the closed-loop thruster dynamics.
3. Implementation of the feedback-linearizing and dead-zone-compensating thruster controller for the six degree-of-freedom (DOF) attitude and velocity setpoint tracking of an ROV with throttle-controlled thruster dynamics.
4. A practical extension of a nonlinear observer previously derived to construct an estimate of the axial fluid velocity through the propeller duct of a thruster. The extension includes considerations for noise present in measurements that were not considered in the design of the original observer. Incorporation of estimates into the dead-zone-compensating controller is addressed for fluid velocity compensation.
5. Experimental evaluation of output feedback control methods using the dead-zone-compensating controller combined with the nonlinear observer, as well as a variant with noise considerations. Thrust tracking performance is compared between controller/estimator combinations based off of different dynamic models.
6. Simulated performance of a full vehicle tracking control scenario using all controller/estimator/model combinations to evaluate the potential benefits of compensating for thruster dynamics with varying levels of complexity.

1.5 Outline of Thesis

The organization of this thesis is as follows. Chapter 2 presents the full six DOF equations of motion for a rigid-body ROV and a feedback-linearizing thrust control law to stabilize the setpoint-tracking dynamics of the system. Chapter 3 discusses modeling and control of the rotor-speed dynamics of the thrusters using a simple dynamic model for nonlinear feedback control. Chapter 4 outlines a more detailed hydrodynamic model for control purposes as well as presents estimation methods to determine the values of unmeasured fluid velocity states. Chapter 5 evaluates the closed-loop performance of previously derived controllers and estimators through experiments as well as simulations and comparisons are made between multiple control strategies. Chapter 6 summarizes the thesis and suggest future work.

Chapter 2: Background: Underwater Vehicle Modeling and Control

This chapter aims to provide necessary background information on underwater vehicle dynamics and control to sufficiently motivate the work in the subsequent chapters. Section 2.1 presents the equations of motion for a generic underwater vehicle and necessary parameters to fully describe motion. Section 2.2 presents a thrust control law to stabilize the closed-loop setpoint-tracking dynamics of an underwater vehicle. The chosen control law for this system is nonlinear in order to guarantee global or nearly global stability, but linear control schemes would also be sufficient. Using such a control law defines a set of desired thrusts that must be achieved by the system actuators, which motivates the analysis of thruster dynamics in later chapters.

2.1 Underwater Vehicle Dynamics

The rigid-body dynamics of an underwater vehicle including hydrodynamic drag and added mass parameters defined in a body-fixed reference frame are typically expressed in terms of matrices and vectors that group common forces and moments. The state vector for these equations is $\mathbf{x} = [x, y, z, \phi, \theta, \psi, u, v, w, p, q, r]^T$ where x , y , and z are Earth-fixed position coordinates, ϕ , θ , and ψ are the 3-2-1 Euler angles

of roll, pitch, and yaw, respectively, and lastly $u, v, w, p, q,$ and r are the respective velocities associated with these degrees of freedom expressed relative to the body frame [36]. It is convenient to separate the states into $\mathbf{x} = [\boldsymbol{\eta}^T \boldsymbol{\nu}^T]^T$ where $\boldsymbol{\eta}$ contains the position and orientation terms and $\boldsymbol{\nu}$ contains the velocity and angular rate terms. The matrix terms include: the rotation and transformation matrix describing linear velocity and attitude rate of the vehicle body-fixed frame relative to the Earth-fixed frame, $J(\boldsymbol{\eta})$, the mass and inertia matrix (including added mass and inertia parameters), M , the nonlinear Coriolis and centripetal matrix, $C(\boldsymbol{\nu})$, the diagonal linear and quadratic hydrodynamic drag matrix, $D(\boldsymbol{\nu})$, and the restoring force and moment vector that combines gravitational and buoyancy effects, $\mathbf{g}(\boldsymbol{\nu})$. Additionally, the external force/moment vector that combines all other effects is denoted as $\boldsymbol{\tau}$ [35]. The equations of motion are then given as [35]

$$\dot{\boldsymbol{\eta}} = J(\boldsymbol{\eta})\boldsymbol{\nu} \quad (2.1)$$

$$M\dot{\boldsymbol{\nu}} = -C(\boldsymbol{\nu})\boldsymbol{\nu} - D(\boldsymbol{\nu})\boldsymbol{\nu} - \mathbf{g}(\boldsymbol{\eta}) + \boldsymbol{\tau}. \quad (2.2)$$

It is useful to separate the states further into 3-element vectors. Let $\boldsymbol{\eta} = [\boldsymbol{\eta}_1^T \ \boldsymbol{\eta}_2^T]^T$ and $\boldsymbol{\nu} = [\boldsymbol{\nu}_1^T \ \boldsymbol{\nu}_2^T]^T$ for $\boldsymbol{\eta}_1 = [x, y, z]^T$, $\boldsymbol{\eta}_2 = [\phi, \theta, \psi]^T$, $\boldsymbol{\nu}_1 = [u, v, w]^T$, and $\boldsymbol{\nu}_2 = [p, q, r]^T$. If absolute position or orientation are not relevant, some or all of the Earth-relative states may be omitted from the full state vector. This work focuses on stabilization of the setpoint-tracking dynamics, where the Earth-relative coordinates $x, y,$ and z are not of interest for the purposes of estimation and control. Therefore, the attitude-only state vector $\boldsymbol{\eta} = \boldsymbol{\eta}_2$ will be used for most descriptions of control

laws in the following sections.

The equations of motion given in (2.1) and (2.2) describe rigid body motion and kinematics supplemented with added mass, drag, buoyancy, and gravitational parameters. To describe the reference frame rotation, the 3-2-1 Euler Angle rotation and transformation matrix $J(\boldsymbol{\eta})$ characterizes the attitude and rotation rate of the body-fixed frame with respect to the Earth-fixed frame, and is given by [35]

$$J(\boldsymbol{\eta}) = \begin{bmatrix} J_1(\boldsymbol{\eta}_2) & 0_{3 \times 3} \\ 0_{3 \times 3} & J_2(\boldsymbol{\eta}_2) \end{bmatrix} \quad (2.3)$$

where the direction cosine matrix $J_1(\boldsymbol{\eta}_2)$ is defined as

$$J_1(\boldsymbol{\eta}_2) = \begin{bmatrix} c\psi c\theta & -s\psi c\phi + c\psi s\theta s\phi & s\psi s\phi + c\psi c\phi s\theta \\ s\psi c\theta & c\psi c\phi + s\phi s\theta s\psi & -c\psi s\phi + s\theta s\psi c\phi \\ -s\theta & c\theta s\phi & c\theta c\phi \end{bmatrix} \quad (2.4)$$

and the angular rate transformation matrix $J_2(\boldsymbol{\eta}_2)$ is

$$J_2(\boldsymbol{\eta}_2) = \begin{bmatrix} 1 & s\phi t\theta & c\phi t\theta \\ 0 & c\phi & -s\phi \\ 0 & s\phi/c\theta & c\phi/c\theta \end{bmatrix}. \quad (2.5)$$

The constant mass and inertia matrix for the equations of motion is typically

represented as a summation of two distinct matrices [35]

$$M = M_{RB} + M_A \quad (2.6)$$

where M_{RB} is the rigid body mass and inertia matrix and M_A is the hydrodynamic added mass and inertia matrix. M_{RB} is written as

$$M_{RB} = \begin{bmatrix} mI_{3 \times 3} & -mS(\mathbf{r}_G) \\ mS(\mathbf{r}_G) & I_G \end{bmatrix}. \quad (2.7)$$

Here, m is the full vehicle mass, and $\mathbf{r}_G = [x_G, y_G, z_G]^T$ is the vector describing the position of the center of mass of the vehicle relative to the body frame (often defined as the origin of the body frame, i.e., $x_G = y_G = z_G = 0$). Additionally, I_G is the inertia matrix defined about the center of gravity

$$I_G = \begin{bmatrix} I_x & -I_{xy} & -I_{xz} \\ -I_{yx} & I_y & -I_{yz} \\ -I_{zx} & -I_{zy} & I_z \end{bmatrix} \quad (2.8)$$

with the moments of inertia about the body axes I_x , I_y , and I_z as well as products of inertia $I_{xy} = I_{yx}$, $I_{xz} = I_{zx}$, and $I_{yz} = I_{zy}$. The skew-symmetric operator $S(\mathbf{x})$ is defined as

$$S(\boldsymbol{\lambda}) = \begin{bmatrix} 0 & -\lambda_3 & \lambda_2 \\ \lambda_3 & 0 & -\lambda_1 \\ -\lambda_2 & \lambda_1 & 0 \end{bmatrix} \quad (2.9)$$

for any 3-element vector $\boldsymbol{\lambda} = [\lambda_1, \lambda_2, \lambda_3]^T$. M_A is typically given as a diagonal matrix of the form

$$M_A = -\text{diag}\{X_{\dot{u}}, Y_{\dot{v}}, Z_{\dot{w}}, K_{\dot{p}}, M_{\dot{q}}, N_{\dot{r}}\} \quad (2.10)$$

where the terms $X_{\dot{u}}$, $Y_{\dot{v}}$, $Z_{\dot{w}}$, $K_{\dot{p}}$, $M_{\dot{q}}$, and $N_{\dot{r}}$ are added mass parameters accounting for the additional mass of water moving with the body, which are typically determined empirically or with computational fluid dynamics (CFD) [36]. Note that under common simplifying cases, M may be diagonal. However, this is greatly dependent on the symmetry of the design of the body, as well as neglecting small off-diagonal terms that may appear in M_A .

The Coriolis and centripetal matrix $C(\boldsymbol{\nu})$ combines nonlinear terms from cross products that arise in the equations of motion. The $C(\boldsymbol{\nu})$ matrix can be represented as a sum of two matrices [35]

$$C(\boldsymbol{\nu}) = C_{RB}(\boldsymbol{\nu}) + C_A(\boldsymbol{\nu}) \quad (2.11)$$

where $C_{RB}(\boldsymbol{\nu})$ is the rigid body Coriolis and centripetal matrix given by

$$C_{RB}(\boldsymbol{\nu}) = \begin{bmatrix} mS(\boldsymbol{\nu}_2) & -mS(\boldsymbol{\nu}_2)S(\mathbf{r}_G) \\ mS(\mathbf{r}_G)S(\boldsymbol{\nu}_2) & -S(I_G\boldsymbol{\nu}_2) \end{bmatrix} \quad (2.12)$$

and the added Coriolis and centripetal matrix C_A can be defined based on portions

of M_A as

$$C_A(\boldsymbol{\nu}) = \begin{bmatrix} 0_{3 \times 3} & -S(A_{11}\boldsymbol{\nu}_1 + A_{12}\boldsymbol{\nu}_2) \\ -S(A_{11}\boldsymbol{\nu}_1 + A_{12}\boldsymbol{\nu}_2) & -S(A_{21}\boldsymbol{\nu}_1 + A_{22}\boldsymbol{\nu}_2) \end{bmatrix} \quad (2.13)$$

for

$$M_A = \begin{bmatrix} A_{11} & A_{12} \\ A_{21} & A_{22} \end{bmatrix}. \quad (2.14)$$

The drag matrix $D(\boldsymbol{\nu})$ can be represented in multiple ways based on the preferred hydrodynamic model. The most common representation defines $D(\boldsymbol{\nu})$ as a summation of both linear and quadratic terms [35]

$$D(\boldsymbol{\nu}) = D_L + D_Q(\boldsymbol{\nu}) \quad (2.15)$$

where

$$D_L = -\text{diag}\{X_u, Y_v, Z_w, K_p, M_q, N_r\} \quad (2.16)$$

and

$$D_Q(\boldsymbol{\nu}) = -\text{diag}\{X_{u|u}|u|, Y_{v|v}|v|, Z_{w|w}|w|, K_{p|p}|p|, M_{q|q}|q|, N_{r|r}|r|\} \quad (2.17)$$

with the parameters $X_u, Y_v, Z_w, K_p, M_q, N_r, X_{u|u}, Y_{v|v}, Z_{w|w}, K_{p|p}, M_{q|q},$ and $N_{r|r}$ determined empirically or through CFD [36].

The effects of restoring forces and moments are typically collected into a single vector of nonlinear terms $\mathbf{g}(\boldsymbol{\eta})$ for convenience. As such, this vector combines gravitational and buoyancy effects in the body-fixed frame. The vector $\mathbf{g}(\boldsymbol{\eta})$ is typically

represented as a combination of rotations and cross products of simple 3-element vectors [35]

$$\mathbf{g}(\boldsymbol{\eta}) = - \begin{bmatrix} \mathbf{f}_G(\boldsymbol{\eta}_2) + \mathbf{f}_B(\boldsymbol{\eta}_2) \\ S(\mathbf{r}_G)\mathbf{f}_G(\boldsymbol{\eta}_2) + S(\mathbf{r}_B)\mathbf{f}_B(\boldsymbol{\eta}_2) \end{bmatrix} \quad (2.18)$$

where the forces due to gravity \mathbf{f}_G and buoyancy \mathbf{f}_B expressed in the body frame are given by

$$\mathbf{f}_G(\boldsymbol{\eta}_2) = J_1^{-1}(\boldsymbol{\eta}_2) \begin{bmatrix} 0 \\ 0 \\ W \end{bmatrix} \quad (2.19)$$

and

$$\mathbf{f}_B(\boldsymbol{\eta}_2) = J_1^{-1}(\boldsymbol{\eta}_2) \begin{bmatrix} 0 \\ 0 \\ -B \end{bmatrix} \quad (2.20)$$

with the forces due to gravity $W = mg$ and buoyancy $B = \rho gV$ where ρ is the density of water, g the acceleration due to gravity, and V the volume of displaced water. Additionally, $\mathbf{r}_B = [x_B, y_B, z_B]^T$ is the position vector of the center of buoyancy expressed in the body frame. Note that in the body and Earth-centered reference frames the force due to gravity is applied in the positive z direction.

The last term to define is the external force and moment vector $\boldsymbol{\tau}$ which collects external forces and moments from currents, thrusters, and other environmental factors. This term will be discussed in the following section for the purposes of control law design.

2.2 Underwater Vehicle Control

The external force/moment vector is treated as the control input, defined as [35]

$$\boldsymbol{\tau} = K_t \mathbf{T}, \quad (2.21)$$

where K_t is the thruster configuration matrix that describes the orientation of each thruster and \mathbf{T} is the vector of input thrusts.

Let $\Delta \boldsymbol{\nu} = \boldsymbol{\nu} - \boldsymbol{\nu}_d$ and $\Delta \boldsymbol{\eta} = \boldsymbol{\eta} - \boldsymbol{\eta}_d$ convert the state-space equations into error coordinates relative to known reference attitude and velocity setpoints $\boldsymbol{\nu}_d$ and $\boldsymbol{\eta}_d$ which are obtainable from user inputs. Also, assume $\dot{\boldsymbol{\nu}}_d$ is readily known and continuous. Martin and Whitcomb [6] then define the following feedback-linearizing control law, assuming perfect knowledge of vehicle states:

$$\begin{aligned} \mathbf{T} = K_t^{-1} [& C(\boldsymbol{\nu})\boldsymbol{\nu} + D(\boldsymbol{\nu})\boldsymbol{\nu} + \mathbf{g}(\boldsymbol{\eta}) + M\dot{\boldsymbol{\nu}}_d \\ & - M(K_P \Delta \boldsymbol{\nu} + K_I(\boldsymbol{\eta}) \Delta \boldsymbol{\eta})], \end{aligned} \quad (2.22)$$

where K_t is assumed to be invertible (or at least has a pseudo inverse). The NGS six-thruster ROV is amenable to this framework.

The integral gain matrix $K_I(\boldsymbol{\eta})$ is a 6×3 matrix varying with vehicle orientation relative to the Earth-fixed frame. The proportional gain matrix K_P is a constant positive-definite symmetric matrix. The control law (2.22) yields the

closed-loop dynamics [6]

$$\frac{d}{dt}(\Delta\boldsymbol{\eta}) = J(\boldsymbol{\eta})\Delta\boldsymbol{\nu} \quad (2.23)$$

$$\frac{d}{dt}(\Delta\boldsymbol{\nu}) = -K_P\Delta\boldsymbol{\nu} - K_I(\boldsymbol{\eta})\Delta\boldsymbol{\eta}, \quad (2.24)$$

which asymptotically stabilize the origin $\Delta\boldsymbol{\eta} = 0$ and $\Delta\boldsymbol{\nu} = 0$ [6].

The control law (2.22) prescribes a set of thrusts that will stabilize the full vehicle setpoint-tracking dynamics. It is common to assume thrusters will rapidly converge to these commanded thrusts using limited knowledge of actuator dynamics, but in the following sections the stability properties of the actuator dynamics will be analyzed. Proper knowledge and control of thruster dynamics will be shown to improve the overall stability properties of the system, and comparison of different models will be carried out to assess the effectiveness of different control schemes.

Chapter 3: Simplified Thruster Modeling and Control

The first set of actuator dynamics that will be analyzed is a simplified model of motor dynamics consisting of a single angular velocity state for a thruster. Such a model assumes a direct, nonlinear mapping from thrust T to propeller angular velocity n . Section 3.1 presents the process for system identification using a six-axis load cell for thrust and torque measurements, then section 3.2 discusses in detail the identified dynamic model. Lastly section 3.3 derives a control law to stabilize the actuator dynamics, which is then extended to prove stability of a full vehicle model when including actuator dynamics. The simplified model is the first in a set of models for actuator dynamics of underwater vehicles, and will be compared to subsequent models in terms of accuracy and benefits of control design in later chapters.

3.1 Experimental Characterization of Model Parameters

3.1.1 Experimental Setup

For system identification of most of the models presented in this and following chapters, a six-axis load cell in a Gough-Stewart platform design (Fig. 3.1) was used

to collect thrust and torque output of an ROV thruster [23]. A six-axis load cell is able to measure forces and moments along three principal axes by utilizing six individual sensors on each of the six rigid arms. The fixed base and attachment platform are connected by the rigid arms with attached axial force sensors (9363-200L-B1-02F, Revere Transducers).

The load cell is configured as two separate plates connected by six legs in a configuration similar to that found on Gough-Stewart manipulators. Fig. 3.2 shows the configuration of the load cell. O is the origin of the reference frame of the system on the fixed upper plate. Forces and moments are applied to the lower platform. It is assumed that there is only a single axial force along each arm and that friction forces are negligible at each joint [23].

Equations to transform the static axial forces along each leg into a resultant force and moment at the origin are well known [34]. Let $\mathbf{f} = [f_1, f_2, f_3, f_4, f_5, f_6]^T$ be

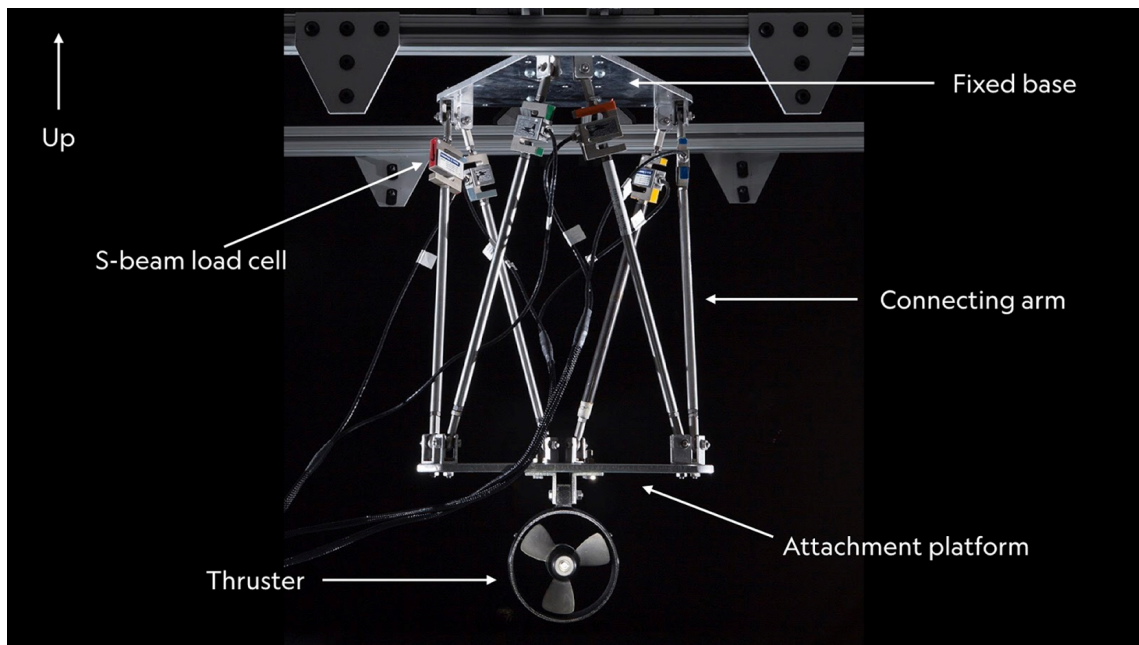


Figure 3.1: Load cell used in model characterization.

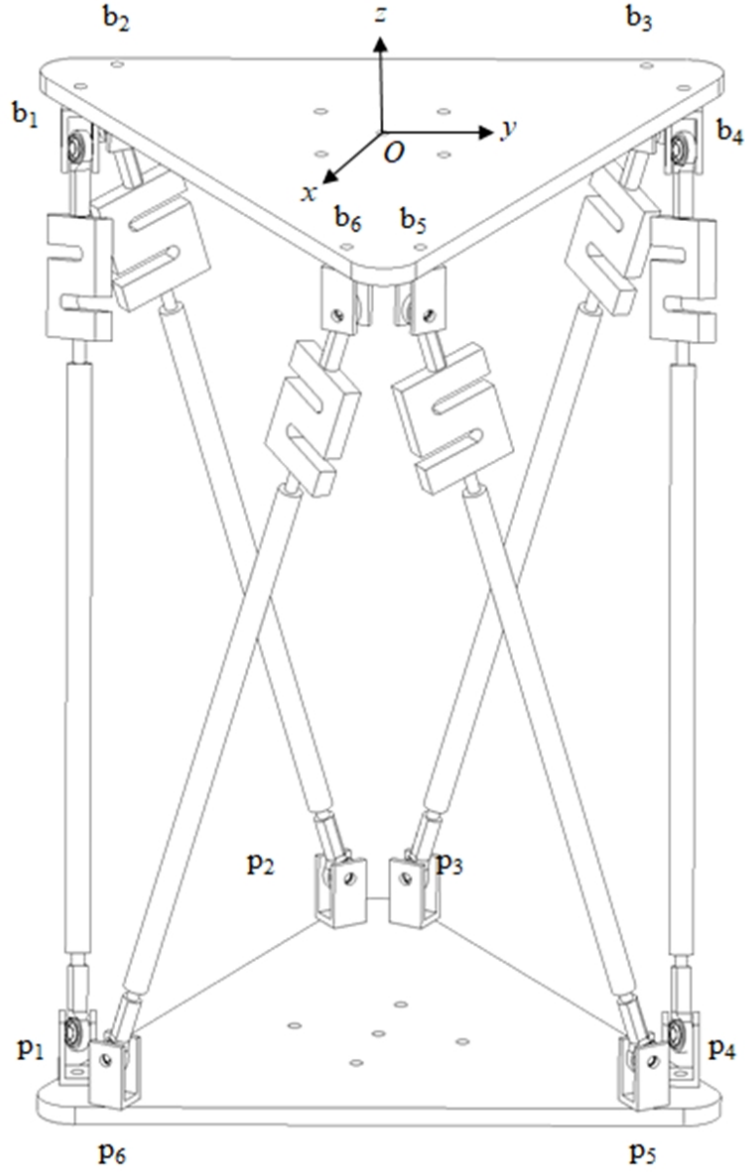


Figure 3.2: Diagram of load cell with principal axes and attachment points marked.

the vector of forces detected along each arm, and let $\mathbf{F}_w = [f_x, f_y, f_z, m_x, m_y, m_z]^T$ the vector of resultant forces f_x, f_y, f_z and moments m_x, m_y, m_z relative to the reference frame of the upper plate. Additionally, let \mathbf{s}_i for $i = 1, \dots, 6$ be the unit vectors defining the orientation of each arm relative to the origin. Intuitively, \mathbf{s}_i should be dependent on the positions of the connection points of each arm to the

top plate \mathbf{b}_i and bottom plate \mathbf{p}_i labeled in Fig. 3.2. This implies the following relation [23]

$$\mathbf{s}_i = \frac{\mathbf{p}_i - \mathbf{b}_i}{\|\mathbf{p}_i - \mathbf{b}_i\|}. \quad (3.1)$$

It follows then that the relation between \mathbf{f} and \mathbf{F}_w based on static equilibrium is [23]

$$\mathbf{F}_w = H\mathbf{f} \quad (3.2)$$

for the transformation matrix H given by

$$H = \begin{bmatrix} \mathbf{s}_1 & \mathbf{s}_2 & \mathbf{s}_3 & \mathbf{s}_4 & \mathbf{s}_5 & \mathbf{s}_6 \\ S(\mathbf{b}_1)\mathbf{s}_1 & S(\mathbf{b}_2)\mathbf{s}_2 & S(\mathbf{b}_3)\mathbf{s}_3 & S(\mathbf{b}_4)\mathbf{s}_4 & S(\mathbf{b}_5)\mathbf{s}_5 & S(\mathbf{b}_6)\mathbf{s}_6 \end{bmatrix}. \quad (3.3)$$

A calibration step was required before using the load cell for system identification of dynamic models. The relation (3.2) is an idealize static model for transforming forces in a rigid structure, but does not take into account mechanical imperfections. Unmodeled errors in the load cell measurements were accounted for by generating an optimal error correction matrix H_E which augments the original transformation matrix H [23]. The augmented transformation matrix $H_A = H + H_E$ replaces H in (3.2). H_E was determined via optimization routines by minimizing residuals of a data set of expected and measured forces. The data were collected by attaching spring scales to the bottom plate in order to apply known loads and measure the resulting forces. By using the relation (3.2), along with data of detected loads $\tilde{\mathbf{f}}$ and knowledge of the applied loads \mathbf{F}_w , the following cost function was used for

optimization

$$J = \|\mathbf{F}_w - H_A \tilde{\mathbf{f}}\|. \quad (3.4)$$

Given that the parameter space for this optimization problem was large, a particle swarm method was used to improve robustness and avoid local minima.

3.1.2 Experimental Procedure

System characterization was performed in a 1 m³ polyethylene water tank. The thruster was provided an analog input signal (-5 V to +5V) using an Agilent 33220 function generator. Time series data of throttle, propeller angular velocity readings (via thruster tachometer), and six load sensor readings were recorded by a data acquisition module (DAQ, USB-6211, National Instruments). A custom LabVIEW application recorded the time series data and performed the transformations (3.2) to provide a time history of the applied forces and moments relative to the load cell reference frame. A block diagram of the test setup is presented in Fig. 3.3 [23]

The system's responses to a series of step inputs at varying voltage levels were recorded to fit both the steady-state and transient responses to models. Steady-state models for thrust T and torque Q as well as a dynamic model for propeller angular velocity n were characterized in these experiments. For all data and models, a Nelder-Mead method of optimization was used to fit the models to the data by minimizing their residuals, which proved sufficient despite the presence of local minima. Identified model fits are compared to data in Fig. 3.4 for steady-state thrust and torque relations, as well as in Fig. 3.5 for transient behavior of thrust, torque,

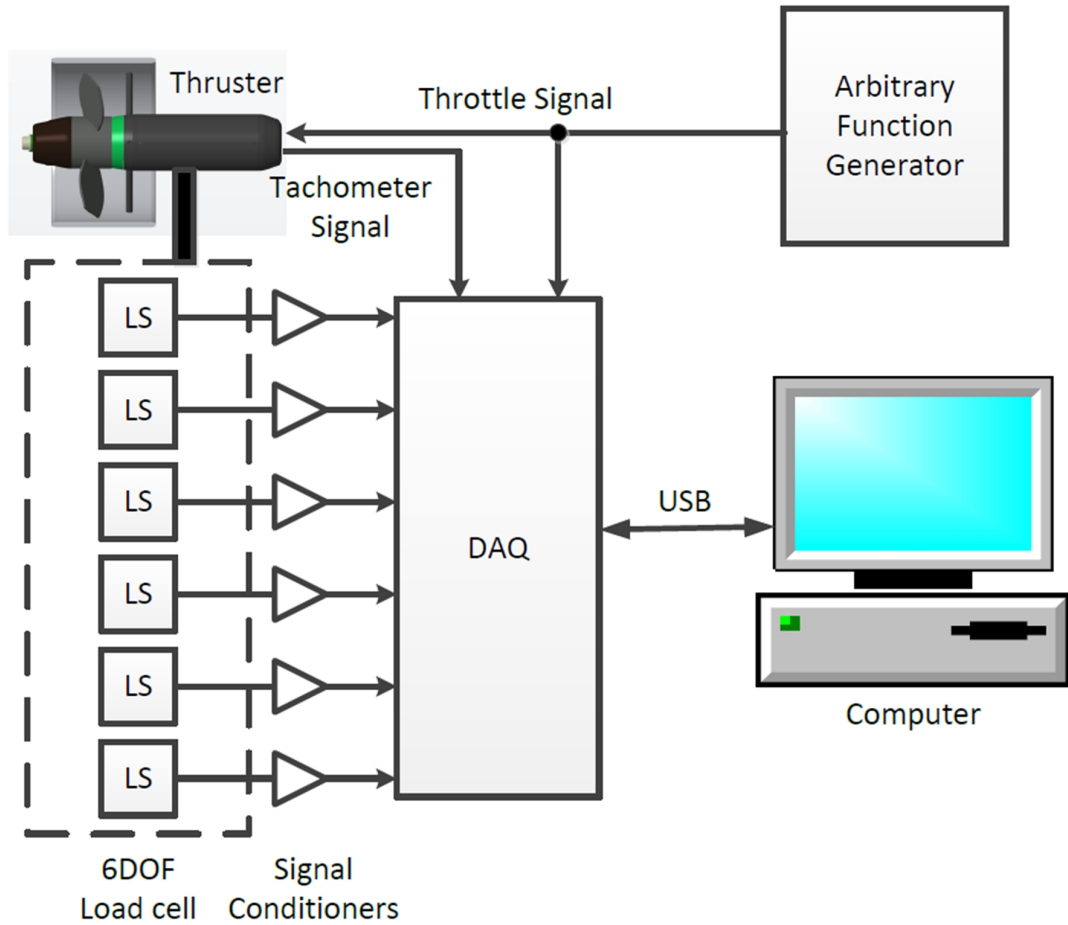


Figure 3.3: Block diagram of experimental data collection system.

and angular velocity. All data were processed through a low-pass filter to remove high-frequency noise. The results show good fits in steady-state and modest fits in transient behavior for thrust and torque despite the well-fit transient behavior in angular velocity. The identified models are discussed in the next section.

3.2 Simplified Thruster Model

The control law in (2.22) defines a desired set of actuator thrusts that stabilize the closed-loop setpoint-tracking dynamics of the ROV. Using data from the

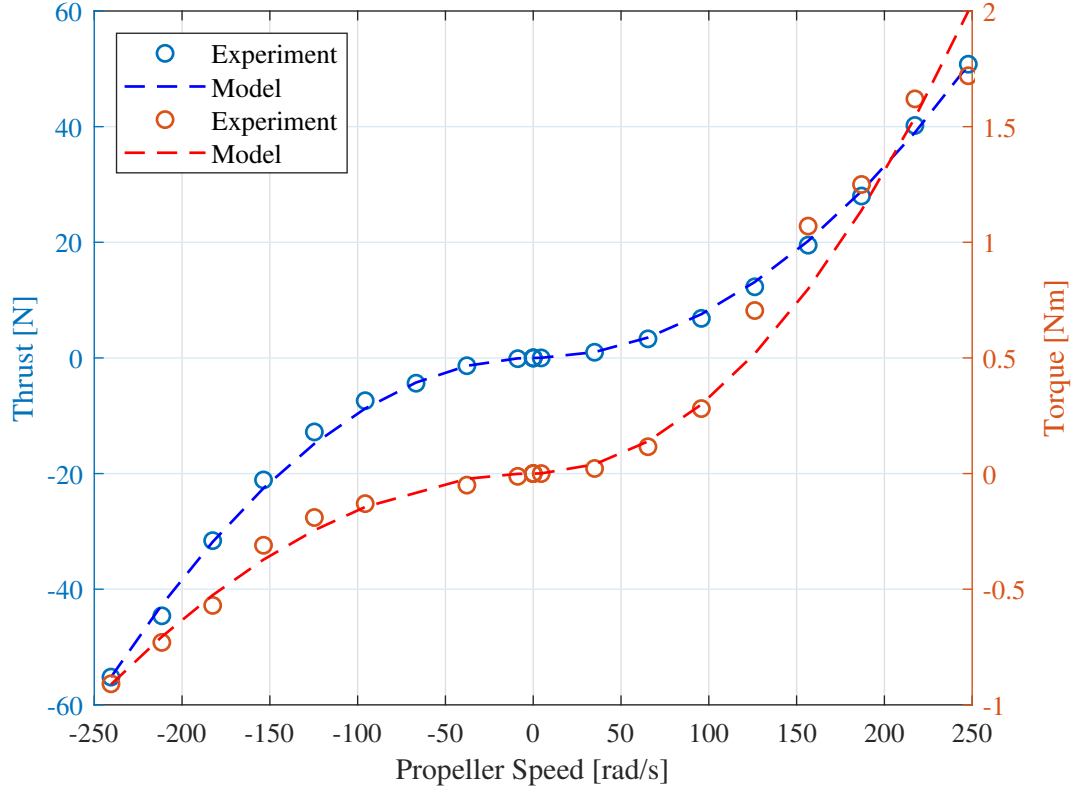


Figure 3.4: Steady-state thrust and torque models compared to experimental data.

previous section, thrust can be related to the propeller angular velocity of an ROV thruster by a quadratic dead zone function [8]

$$T(n) = \begin{cases} c_{T1}(n|n| - \delta_{T1}), & n|n| \leq \delta_{T1} \\ 0, & \delta_{T1} < n|n| < \delta_{T2} \\ c_{T2}(n|n| - \delta_{T2}), & n|n| \geq \delta_{T2}, \end{cases} \quad (3.5)$$

where n represents propeller angular velocity, the constants c_{T1} , c_{T2} , and δ_{T2} are positive, and δ_{T1} is negative. In order to determine the desired propeller angular

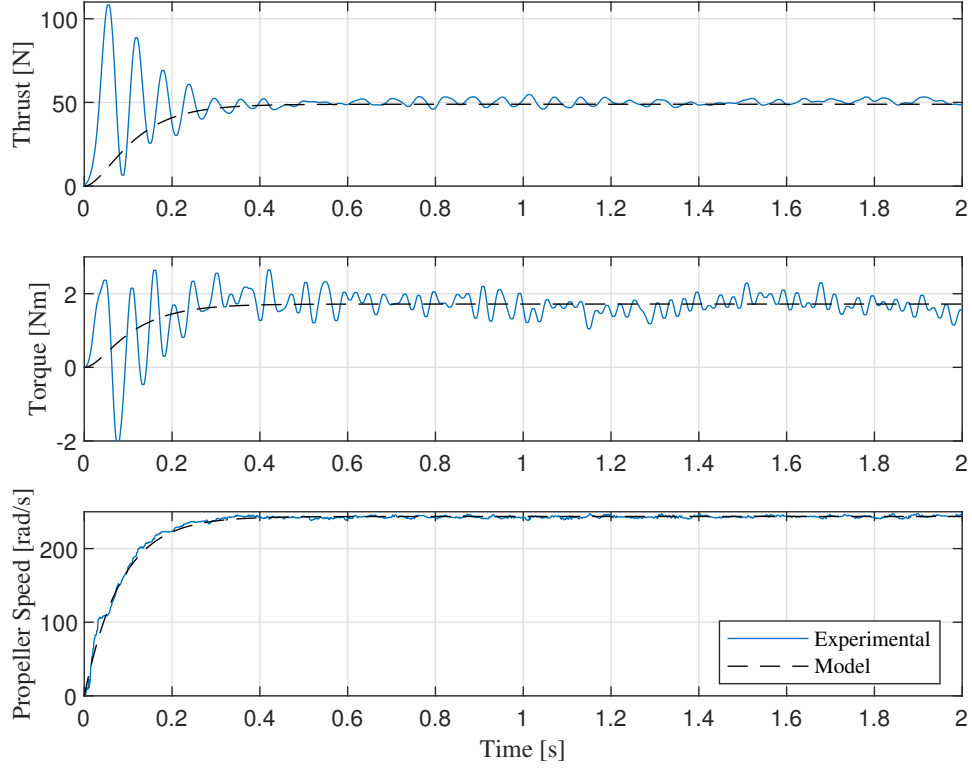


Figure 3.5: Step responses of thrust, torque, and rotor speed models compared to experimental data.

velocity n_d for a desired thrust T_d , inverting the dead zone function (3.5) yields [8]

$$n_d = \begin{cases} \operatorname{sgn}(T_d) \sqrt{\left| \frac{T_d}{c_{T1}} + \delta_{T1} \right|}, & T_d < 0 \\ 0, & T_d = 0 \\ \operatorname{sgn}(T_d) \sqrt{\left| \frac{T_d}{c_{T2}} + \delta_{T2} \right|}, & T_d > 0. \end{cases} \quad (3.6)$$

The desired propeller angular velocity n_d is then usable as a setpoint to be fed back into a control scheme for the actuator dynamics. Bessa et al. [8] propose the

following voltage-driven dynamic model for an ROV thruster:

$$\dot{n} = -k_1 n - k_2 n |n| + k_3 u, \quad (3.7)$$

where u is the input motor voltage and the constants k_1 , k_2 , and k_3 are positive. Equation (3.7) is a single-state thruster model that is valid at low propeller speeds [8].

This work considers an alternate version of (3.7) that, instead of being driven by a direct motor voltage, is controlled by an analog voltage throttle signal with a dead zone around zero volts. The new model is [19]

$$\dot{n} = -k_n n - k_Q Q(n) + \gamma(u), \quad (3.8)$$

where $Q(n)$ is the reaction torque on the propeller, and the function $\gamma(u)$ relates throttle signal u to motor torque by a linear dead zone function [19]

$$\gamma(u) = \begin{cases} c_{u1}(u - \delta_{u1}), & u \leq \delta_{u1} \\ 0, & \delta_{u1} < u < \delta_{u2} \\ c_{u2}(u - \delta_{u2}), & u \geq \delta_{u2}. \end{cases} \quad (3.9)$$

The effects of the nonlinear function (3.9) on (3.8) are presented in Fig. 3.6 by plotting steady-state propeller speed data as a function of the constant throttle voltages that drive the system to those operating points. A fit based on (3.8) is also

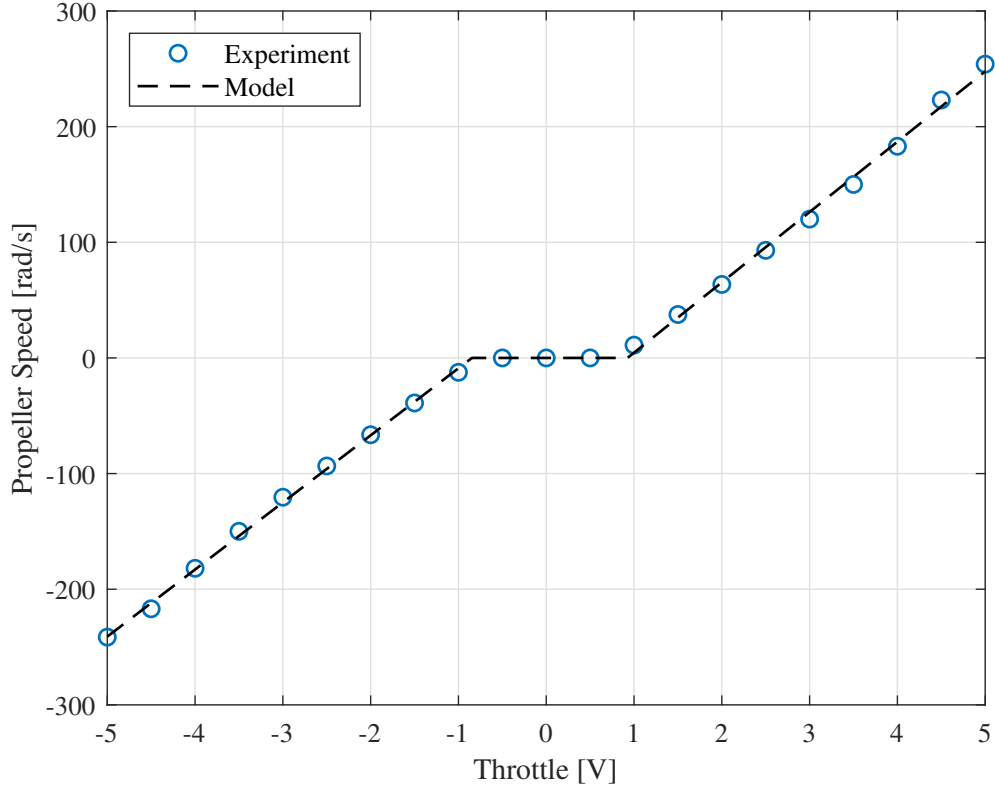


Figure 3.6: Steady-state propeller angular velocity data.

plotted to validate the accuracy of the model. Note that (3.9) can be inverted as

$$\gamma^{-1}(\alpha) = \begin{cases} c_{u1}^{-1}\alpha + \delta_{u1}, & \alpha < 0 \\ 0, & \alpha = 0 \\ c_{u2}^{-1}\alpha + \delta_{u2}, & \alpha > 0, \end{cases} \quad (3.10)$$

for any generic commanded motor torque α .

In (3.8), Q represents the collected inertial and hydrodynamic reaction torque enacted on the thrusters, which is often a quadratic function of n , and may be

defined with a dead zone similar to (3.5), i.e.,

$$Q(n) = \begin{cases} c_{Q1}(n|n| - \delta_{Q1}), & n|n| \leq \delta_{Q1} \\ 0, & \delta_{Q1} < n|n| < \delta_{Q2} \\ c_{Q2}(n|n| - \delta_{Q2}), & n|n| \geq \delta_{Q2}, \end{cases} \quad (3.11)$$

with positive constants c_{Q1} , c_{Q2} , and δ_{Q2} , and negative constant δ_{Q1} . Identified values of parameters for the defined models (3.5), (3.8), (3.9), and (3.11) are reported in Table 3.1.

Table 3.1: Simplified Model Parameter Values

Parameter	Value	Units
c_{T1}	9.548×10^{-4}	$\text{N} \cdot \text{s}^2$
c_{T2}	8.248×10^{-4}	$\text{N} \cdot \text{s}^2$
δ_{T1}	-0.032	s^{-2}
δ_{T2}	2.187×10^{-3}	s^{-2}
c_{Q1}	1.577×10^{-5}	$\text{N} \cdot \text{m} \cdot \text{s}^2$
c_{Q2}	3.255×10^{-5}	$\text{N} \cdot \text{m} \cdot \text{s}^2$
δ_{Q1}	-0.0215	s^{-2}
δ_{Q2}	0.0192	s^{-2}
c_{u1}	793.6	$(\text{V} \cdot \text{s}^2)^{-1}$
c_{u2}	709	$(\text{V} \cdot \text{s}^2)^{-1}$
δ_{u1}	-0.8475	V
δ_{u2}	0.9254	V
k_n	11.30	s^{-1}
k_Q	67.66	$(\text{N} \cdot \text{m} \cdot \text{s}^2)^{-1}$
\dot{u}_{max}	100	$\text{V} \cdot \text{s}^{-1}$

3.3 Feedback Control Strategy

3.3.1 Single-Thruster Control

To drive the dynamics (3.8) to a known setpoint n_d , a nonlinear control strategy is necessary. Using the inverse dead zone function (3.10) and feedback linearization, a control law that compensates for nonlinearities in the thruster dynamics is derived. This framework is shown below to exponentially stabilize $n = n_d$.

Theorem 1. *Assuming u can change instantaneously, the dynamics (3.8) exponentially stabilize the setpoint $\Delta n = n - n_d = 0$ using the control law*

$$u = \gamma^{-1}(\alpha), \quad (3.12)$$

where $\gamma^{-1}(\alpha)$ is defined in (3.10) and

$$\alpha = \dot{n}_d + k_n n + k_Q Q(n) - k_u \Delta n, \quad (3.13)$$

for $k_u > 0$.

Proof. Consider the scenario where the system is operating under the first condition in (3.10), i.e., $\alpha < 0$. Therefore, (3.8) becomes

$$\begin{aligned} \dot{n} &= -k_n n - k_Q Q(n) + k_{u1}(k_{u1}^{-1} \alpha + \delta_{u1} - \delta_{u1}) \\ &= -k_n n - k_Q Q(n) + \dot{n}_d + k_n n + k_Q Q(n) - k_u \Delta n \\ &= \dot{n}_d - k_u \Delta n, \end{aligned} \quad (3.14)$$

which implies

$$\frac{d}{dt}(\Delta n) = -k_u \Delta n. \quad (3.15)$$

Equation (3.15) is a scalar Hurwitz linear system in error coordinates relative to the setpoint n_d .

The same steps yield identical results for the third condition of (3.10), so operating on either end of the dead zone yields the system (3.15). In the case that $\alpha = 0$, substituting (3.13) into (3.8) yields

$$\begin{aligned} \dot{n} &= -k_n n - k_Q Q(n) \\ &= -\alpha + \dot{n}_d - k_u \Delta n \\ &= \dot{n}_d - k_u \Delta n, \end{aligned} \quad (3.16)$$

which is the same result as (3.15) and therefore completes the proof. \square

If perfect knowledge of \dot{n}_d is not available in practice, a piecewise constant estimate may be used in its place. The following result is obtained in the presence of inaccurate estimates of \dot{n}_d .

Corollary 1.1. *Let $\delta > 0$. Using the estimate $\tilde{\dot{n}}_d = \dot{n}_d + \epsilon$, where the estimation error ϵ satisfies $|\epsilon| < \delta$, the solution to the closed-loop dynamics (3.15) using the control law (3.12) is bounded by $|\Delta n| \leq \delta/k_u$.*

Proof. With the estimate $\tilde{\dot{n}}_d = \dot{n}_d + \epsilon$, (3.15) becomes

$$\frac{d}{dt}(\Delta n) = -k_u \Delta n + \epsilon. \quad (3.17)$$

Consider the quadratic Lyapunov function

$$V = \frac{1}{2}(\Delta n)^2, \quad (3.18)$$

whose time-derivative along solutions of (3.17) satisfies

$$\begin{aligned} \dot{V} &= -k_u(\Delta n)^2 + \Delta n \epsilon \\ &\leq -k_u(\Delta n)^2 + |\Delta n|\delta, \end{aligned} \quad (3.19)$$

which implies the closed-loop dynamics (3.15) converge to $|\Delta n| \leq \delta/k_u$. \square

In practice, physical thrusters have a maximum ramp speed, i.e., u cannot change instantaneously, which limits the convergence rate to the desired setpoint. This limitation is modeled as a maximum allowable throttle change rate, i.e., \dot{u}_{max} . Since u cannot change instantaneously, it may pass through the dead zone. The maximum amount of time the motor spends in the dead zone while transitioning to a thruster operating point outside the dead zone is [19]

$$t_{max} = \frac{\delta_{u2} - \delta_{u1}}{\dot{u}_{max}} > 0. \quad (3.20)$$

During this time, the dynamics (3.8) will be unforced, requiring additional analysis of the system in this scenario.

Theorem 2. *Consider the dynamics (3.8). When u is within the throttle dead zone, the zero-input dynamics*

$$\dot{n} = -k_n n - k_Q Q(n) \quad (3.21)$$

exponentially stabilize the origin $n = 0$.

Proof. The stability properties of the unforced system (3.21) can be analyzed with the quadratic Lyapunov function

$$V = \frac{1}{2}n^2, \quad (3.22)$$

which varies according to

$$\dot{V} = -k_n n^2 - k_q Q(n)n. \quad (3.23)$$

Equation (3.23) can take one of three forms depending on the value of n . Because the constants k_n and k_q are positive, \dot{V} is negative definite if $Q(n)n$ is positive semi-definite for all n . According to (3.11), $Q(n)$ either has the same sign as n or is zero for $\delta_{Q1} < n|n| < \delta_{Q2}$, because c_{Q1} , c_{Q2} , and δ_{Q2} are all positive and δ_{Q1} is negative. $Q(n)n$ is therefore positive semi-definite, and \dot{V} is negative definite for all n . Note that $k_a n^2 \leq V \leq k_b n^2$ and $\dot{V} \leq -k_n n^2$ for $k_b > 0.5 > k_a > 0$, which implies that the unforced system (3.21) exponentially stabilizes the origin. \square

The thruster motor operates in the dead zone in one of only three scenarios: during startup, wind-down, or a transition between forward and reverse thrust. In all of these scenarios, convergence to zero propeller speed is either advantageous or inconsequential (as in the case of motor startup). Typically t_{max} in (3.20) is on the order of tens of milliseconds, whereas the wind-down time for an ROV thruster was experimentally observed to be as much as half a second [23]. As a result, crossing

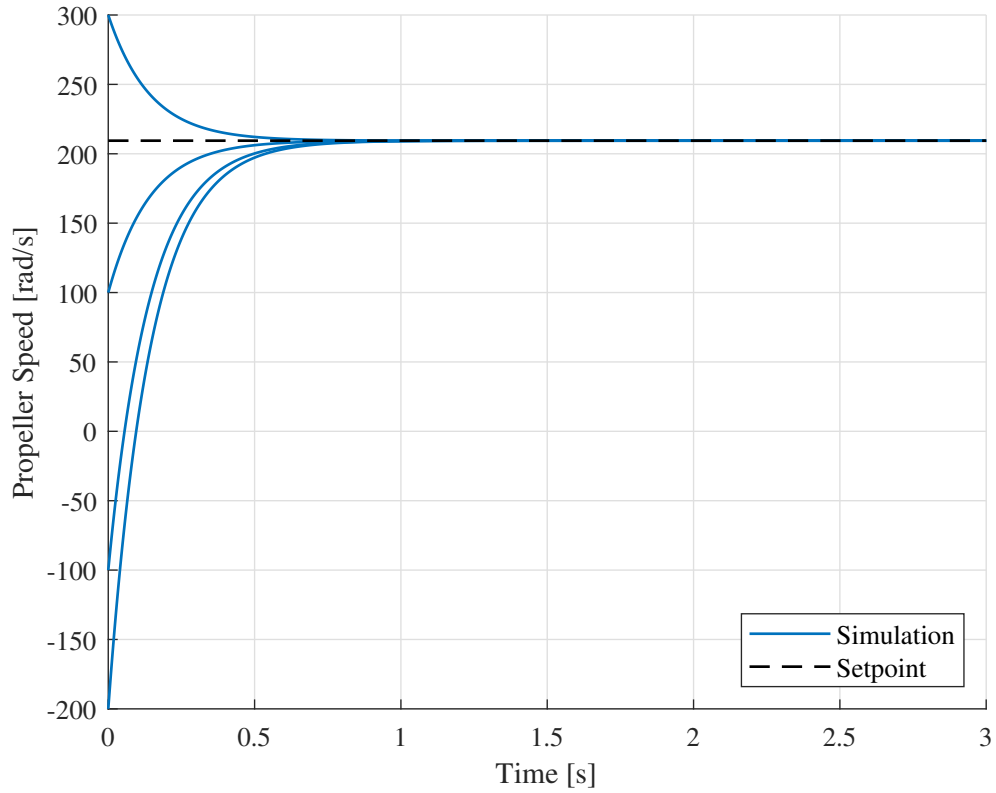


Figure 3.7: Control simulations driving a thruster to a setpoint n_d with consideration for \dot{u}_{max} .

the throttle dead zone is not predicted to destabilize the physical system during regular operation. Fig. 3.7 depicts a simulation of the dead-zone-compensating controller (3.12) successfully driving the actuator dynamics from multiple operating points of n to a positive setpoint value of n_d , taking into account the limitation $|\dot{u}| \leq \dot{u}_{max}$.

3.3.2 Full Vehicle Control

The preceding analysis for a single thruster system can be reasonably extended to a multi-thruster system with full vehicle dynamics as thruster dynamics are gen-

erally uncoupled. The systems in (2.1), (2.2), and (3.8) represent the full system dynamics of the ROV, including rigid-body dynamics and uncoupled actuator dynamics for each thruster, i.e.,

$$\dot{\mathbf{x}} = \mathbf{f}(\mathbf{x}) + \mathbf{g}(\mathbf{u}), \quad (3.24)$$

where $\mathbf{x} = [\boldsymbol{\eta}^T \boldsymbol{\nu}^T \mathbf{n}^T]^T$ and \mathbf{n} is the vector of the (six) thruster states of the ROV.

The vector fields $\mathbf{f}(\mathbf{x})$ and $\mathbf{g}(\mathbf{u})$ are [19]

$$\mathbf{f}(\mathbf{x}) = \begin{bmatrix} J(\boldsymbol{\eta})\boldsymbol{\nu} \\ M^{-1}[K_t\mathbf{T}(\mathbf{n}) - C(\boldsymbol{\nu})\boldsymbol{\nu} - D(\boldsymbol{\nu})\boldsymbol{\nu} - \mathbf{g}(\boldsymbol{\eta})] \\ -K_n\mathbf{n} - K_Q\mathbf{Q}(\mathbf{n}) \end{bmatrix}, \quad (3.25)$$

and

$$\mathbf{g}(\mathbf{u}) = \begin{bmatrix} 0 \\ \vdots \\ 0 \\ \boldsymbol{\gamma}(\mathbf{u}) \end{bmatrix} \quad (3.26)$$

where K_n and K_Q are diagonal matrices containing the parameters of the dynamics from (3.8) for each individual thruster. The closed-loop dynamics take the form

$$\frac{d}{dt} \begin{bmatrix} \Delta\boldsymbol{\eta} \\ \Delta\boldsymbol{\nu} \\ \Delta\mathbf{n} \end{bmatrix} = \begin{bmatrix} J(\boldsymbol{\eta})\Delta\boldsymbol{\nu} \\ -K_P\Delta\boldsymbol{\nu} - K_I(\boldsymbol{\eta})\Delta\boldsymbol{\eta} \\ -K_u\Delta\mathbf{n} \end{bmatrix} \quad (3.27)$$

where K_u is the diagonal matrix of feedback gains.

Theorem 3. *The full closed-loop dynamics for the ROV (3.27) asymptotically stabilize the origin $\Delta \mathbf{x} = \mathbf{x} - \mathbf{x}_d = 0$.*

Proof. The system (3.27) combines the dynamics in (2.1) and (2.2), which asymptotically stabilize the origin $\Delta \boldsymbol{\nu} = 0$ and $\Delta \boldsymbol{\eta} = 0$, with the dynamics of the thrusters (3.8) which are fully uncoupled and each exponentially stabilize the origin $\Delta \mathbf{n} = 0$. Therefore, because each sub-system is asymptotically stable, the full closed-loop system asymptotically stabilizes the origin $\Delta \mathbf{x} = 0$. \square

Experimental validation of the control methods outlined in this section as well as comparisons of simulated performance of these methods applied to a full vehicle model are discussed in later chapters.

Chapter 4: Hydrodynamic Thruster Modeling and Control

Newer work in dynamic modeling of underwater vehicle thrusters has focused on expanding model dimensionality to describe the effects of fluid interaction on thrust generation. As the focus of controlling actuator dynamics for underwater vehicles is closing the loop on thrust rather than angular velocity, implementing model-based control strategies for more accurate models of thrust is a natural next step in this analysis. The dynamic models presented in previous sections are therefore augmented with new states that characterize the time evolution of fluid velocity and how resulting hydrodynamic forces generate thrust losses [12]. This chapter goes about describing these models and their uses in actuator control by first outlining the experimental methods used to characterize them in section 4.1. The new models are then described in section 4.2. From there, section 4.3 discusses nonlinear estimation methods used to construct estimates of unmeasured states, and then section 4.4 outlines how to use knowledge of the expanded state space to improve previously discussed feedback control strategies.

4.1 Experimental Characterization of Model Parameters

4.1.1 Experimental Setup

The process of augmenting the previously discussed actuator dynamics allows the preservation of previously discussed system identification methods. This eases further model characterization tasks as the procedure remains mostly unchanged. The same six-axis load cell could therefore be reused for characterization tests. However, the previous data collection method and test tank did not allow for fluid velocity measurements. Therefore a new test tank that did not restrict fluid flow as well as a flow meter were necessary to make such measurements.

Experimentally, a Nortek Vectrino model ADV was used to collect fluid velocity time-series measurements at 25 Hz. ADVs are well-documented, reliable devices for the purpose of fluid model characterization [13, 17]. These measurements were used for both model characterization and in closed-loop output feedback experiments discussed in following chapters. All experiments were performed in a Loligo Systems flow tank with a 25×25 cm cross section where the thruster drives the fluid velocity of the tank and force measurements are again obtained by a six-axis load cell [23]. All other aspects of the experimental setup remain unchanged from Section 3.1. The experimental setup with the ADV and load cell is depicted in Fig. 4.1.

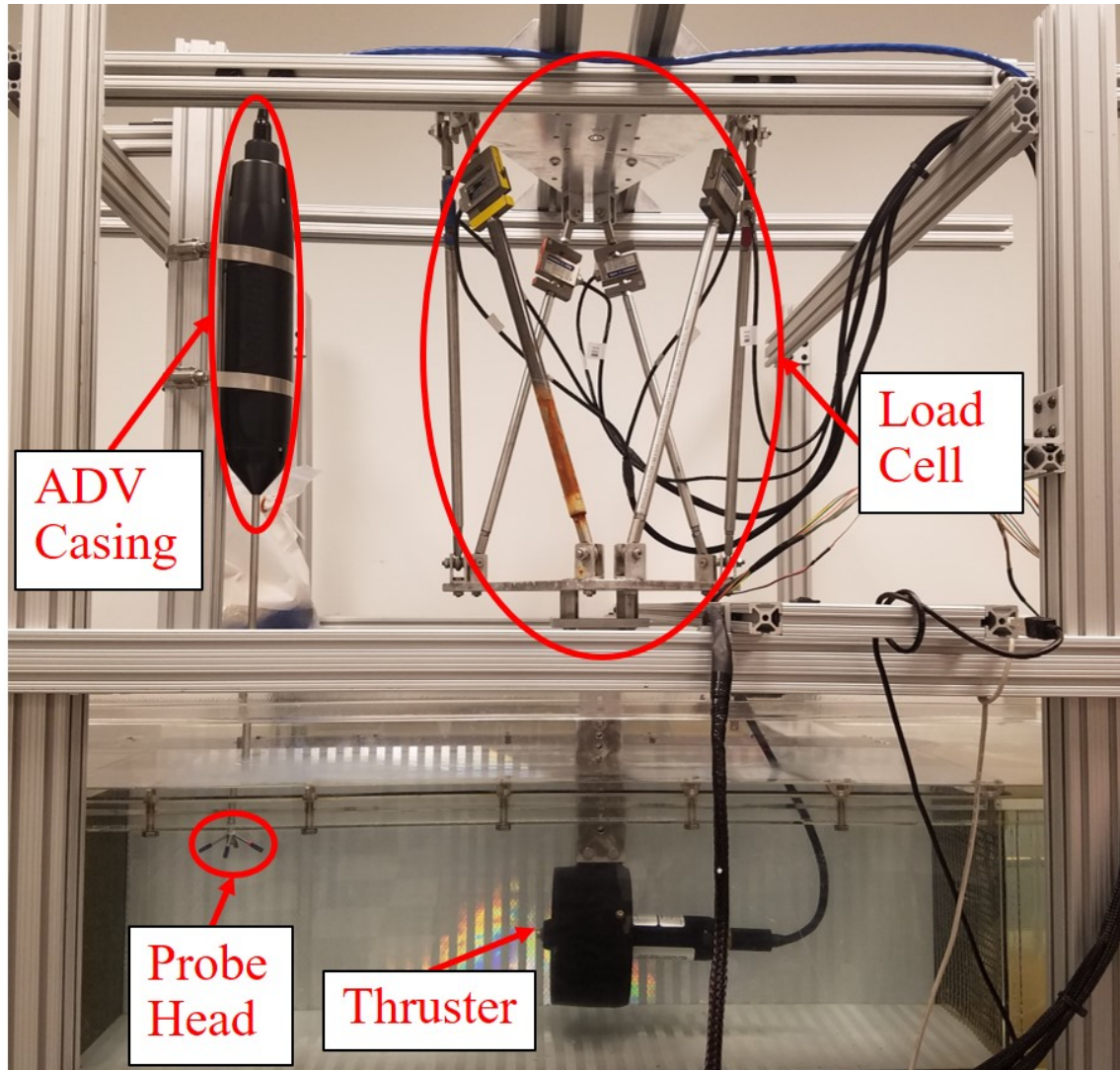


Figure 4.1: Annotated image of experimental setup with load cell and ADV used in model characterization.

4.1.2 Experimental Procedure

All data were collected as time-series responses to a transient input ramp over two seconds followed by a constant input over eight seconds to allow the subsequent steady-state behavior to be captured. For all experiments, data were collected for axial thrust, torque, propeller angular velocity, and fluid velocity. Data were collected for steady-state inputs ranging from -3 V to $+3\text{ V}$, which is a smaller range

than previous experiments. This is due to restrictions of the flow tank for turbulent flow, as higher operating speeds of the thruster induce waves and cavitation that interfere with sensor measurements and data quality. Additionally, all of the experiments were run for two different flow-sensing scenarios: once for collecting ambient velocity data at a distance from the thruster duct, and again for axial velocity data directly in front of the thruster duct. These two data sets were necessary as the thruster was capable of driving the fluid flow through the tank which in turn directly affected fluid velocity behavior in front of the thruster duct.

Steady-state relations for thrust and torque were again characterized as well as dynamic models for propeller angular velocity, axial fluid velocity, and ambient fluid velocity. Nelder-Mead optimizations were implemented just as before to fit the models to the data by minimizing residuals. Identified model fits are compared to data in Fig. 4.2 for all measurement methods in a representative set of experiments. Each measurement is shown in response to ± 3 V steady-state inputs after a two second ramp to that operating point. Transients and steady-state behavior were fit well to the models outlined in the following section.

4.2 Hydrodynamic Thruster Model

A hydrodynamic model of thruster performance is common and well documented, even though model choices have varied over time [11–13, 16, 18, 38]. Typically two forms of fluid velocity are accounted for in dynamic modeling: the axial fluid velocity across the propeller disc v , and the ambient velocity of the surround-

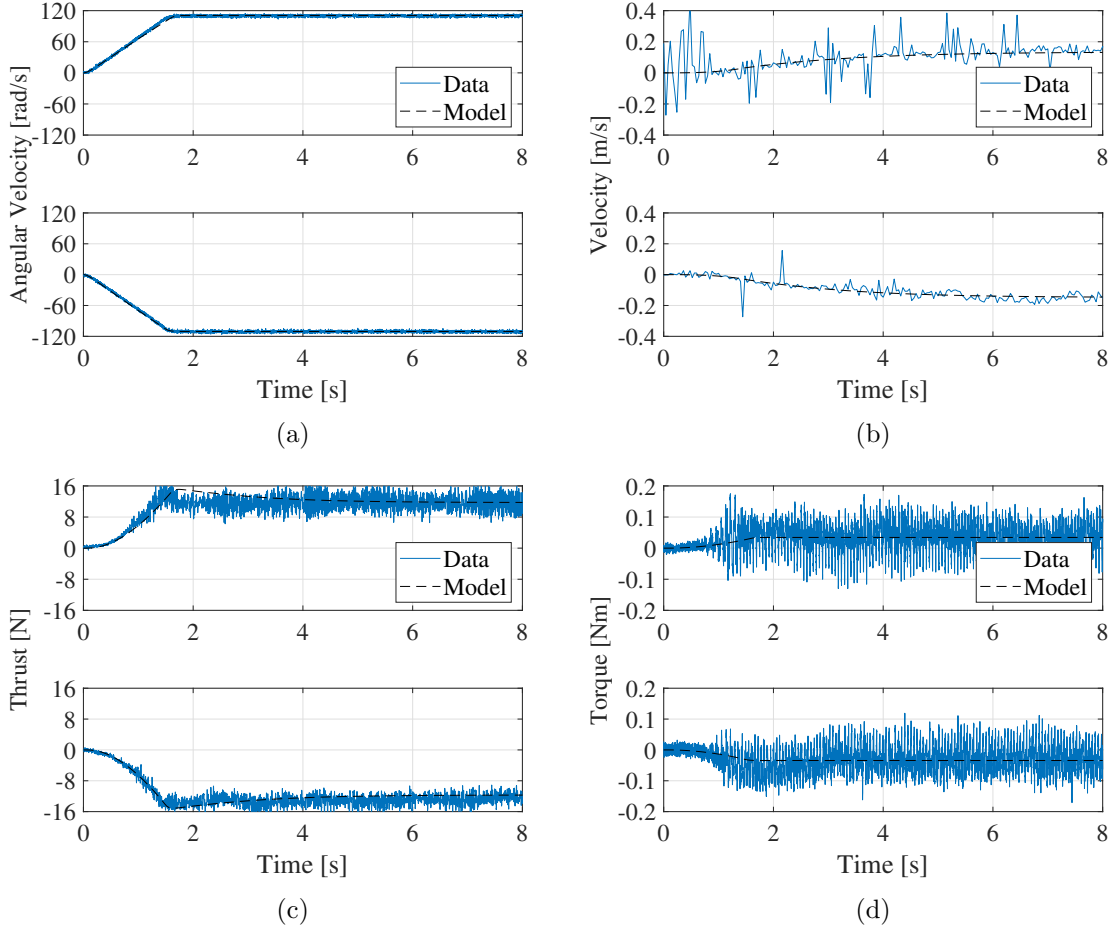


Figure 4.2: Model fit results from system identification procedures done for hydrodynamic thruster models. Fits shown for (a) angular velocity, (b) fluid velocity, (c) thrust, and (d) torque.

ing water U . The interactions between these two velocities and propeller angular velocity can be modeled both dynamically and via static relations. Healy et al. [11] propose a two-state dynamic model that combines angular velocity dynamics similar to (3.8) with axial velocity dynamics driven by the resultant thrust and ambient velocity that is assumed to be a uniform freestream value:

$$\dot{n} = -k_1 n - k_2 Q(n, v) + k_3 u \quad (4.1)$$

$$\dot{v} = -k_4 (v - U) |v - U| + k_5 T(n, v). \quad (4.2)$$

The parameters $k_1, k_2, k_3, k_4,$ and k_5 are positive. It should be noted that regardless of model, v and U are assumed uniform.

Other work assumes a dynamic model for U which is more representative of the dynamics for underwater vehicles being propelled by aquatic thrusters [12, 16, 18, 38]. Kim and Chung [16] define v as a linear combination of U and n assuming a steady flow relationship. To account for more complicated interactions, this work uses a model first presented by Blanke et al. [12] that includes both fluid velocities in the state-space:

$$\dot{n} = -k_n n - k_Q Q(n, v) + \gamma(u) \quad (4.3)$$

$$\dot{v} = -k_v v - k_{Uv} |v| (v - k_w U) + k_{Tv} T(n, v) \quad (4.4)$$

$$\dot{U} = -k_U U - k_{UU} U |U| + k_{TU} T(n, v). \quad (4.5)$$

Here $\gamma(u)$ is used to represent a more general input torque function, but in subsequent analysis will be assumed to represent the nonlinear dead zone function (3.9). It should be noted that all coefficients in this model are defined as positive constants. This dynamic model is advantageous for its more general representation of the fluid velocities, as U can represent the forward speed of a single-thruster vehicle or the fluid velocity in a flow tank. A diagram depicting all the relevant quantities in this dynamic system as they relate physically to an aquatic thruster is presented in Fig 4.3.

An important factor in improving model fidelity is how the mappings for thrust and torque are defined. Healey et al. [11] as well as Bachmayer et al. [13] both use

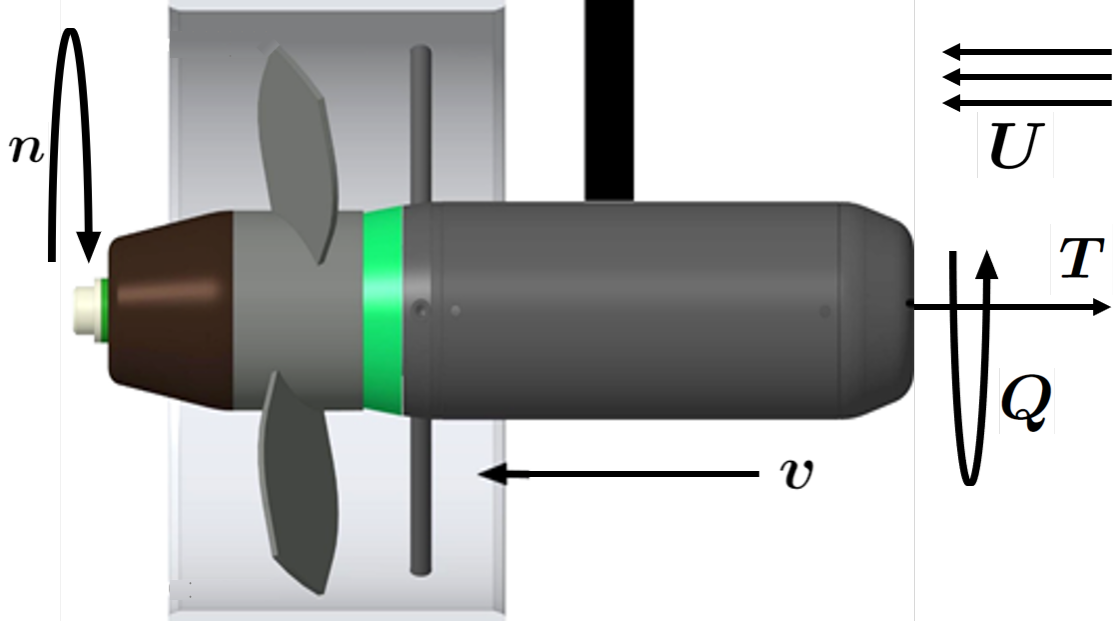


Figure 4.3: Diagram of how physically relevant values in thruster models relate to the thruster system.

airfoil theory to define physically meaningful mappings for $T(n, v)$ and $Q(n, v)$ based on sinusoidal lift and drag coefficients:

$$T(n, v) = L(n, v) \cos \theta - D(n, v) \sin \theta \quad (4.6)$$

$$Q(n, v) = 0.7R(L(n, v) \sin \theta + D(n, v) \cos \theta) \quad (4.7)$$

$$L(n, v) = 0.5\rho\pi R^2 V^2 C_{L_{max}} \sin(2(p - \theta)) \quad (4.8)$$

$$D(n, v) = 0.5\rho\pi R^2 V^2 C_{D_{max}} (1 - \cos(2(p - \theta))) \quad (4.9)$$

where

$$\theta = \text{atan2}(v, 0.7Rn) \quad (4.10)$$

$$V^2 = v^2 + (0.7Rn)^2. \quad (4.11)$$

The parameters for propeller blade pitch angle p , propeller disc radius R , as well as maximum lift and drag coefficients $C_{L_{max}}$, and $C_{D_{max}}$ are specific parameters of the physical system and must be manually measured or experimentally determined, and ρ represents the density of water [11, 17, 39]. While such rigorous models are attractive for their ability to accurately describe the physical system, they can overly complicate practical control strategies, and have demonstrated inconsistencies with experimentally observed performance [13, 17].

In contrast to the detailed and highly nonlinear models (4.6) and (4.7), more recent work utilizes heuristic models that forgo accuracy to hydrodynamic theory for more tractable relations of $T(n, v)$ and $Q(n, v)$ [12, 16]. Blanke et al. [12] define $T(n, v)$ and $Q(n, v)$ as nonlinear mappings based on steady-state data:

$$T(n, v) = c_n^T n |n| - c_{nv}^T |n|v \quad (4.12)$$

$$Q(n, v) = c_n^Q n |n| - c_{nv}^Q |n|v \quad (4.13)$$

where c_n^T , c_{nv}^T , c_n^Q , and c_{nv}^Q are positive. The dependence on v in these equations therefore models thrust and torque losses due to fluidic effects [18]. Note that this model is similar to (3.5) and (3.11) but without considerations for asymmetric behavior between positive and negative values of n . This makes the model simpler and more tractable for estimation and control analysis. The equations of motion (4.3), (4.4), and (4.5) when using these mappings for $T(n, v)$ and $Q(n, v)$ will be referred to as a hydrodynamic linear (HL) model because of its purely linear dependence on v .

Besides being heuristically defined relations, the models for thrust and torque

in (4.12) and (4.13) are considered simplified expressions due to their linear dependence on v . More recent work suggests that a *quadratic* relation with v more accurately models steady-state behavior and has been verified experimentally [16]. Kim and Chung [16] propose the following model as an improvement on the HL equations (4.12) and (4.13):

$$T(n, v) = c_n^T n |n| - c_{nv}^T |n|v - c_v^T v |v| \quad (4.14)$$

$$Q(n, v) = c_n^Q n |n| - c_{nv}^Q |n|v - c_v^Q v |v| \quad (4.15)$$

where the additional parameters c_v^T and c_v^Q are also positive. Including these extra terms more accurately represents the nonlinear behavior of thrust and torque at varying values of v , especially when the signs of v and n oppose one another [16]. The model presented in (4.3), (4.4), and (4.5) when using this relation will be referred to as a hydrodynamic quadratic (HQ) model due to the quadratic dependence on v .

While the HQ expressions (4.14) and (4.15) offer more accurate descriptions of nonlinearities in thrust and torque behavior due to fluidic effects, the HL model can still be effective in approximating hydrodynamic losses in these quantities [18]. In addition, the simpler form of (4.12) and (4.13) enables stronger convergence guarantees for the estimation methods discussed in the next section [18]. Both hydrodynamic models will be used experimentally and in simulation in the next chapter to evaluate the performance improvement of model-based control. Table 4.1 reports identified parameters for the aforementioned models. In addition, table 4.2 presents values specific to the two hydrodynamic models for $T(n, v)$ and $Q(n, v)$.

Table 4.1: Hydrodynamic Model Parameter Values

Parameter	Value	Units
c_{u1}	725.5	$(\text{V}\cdot\text{s}^2)^{-1}$
c_{u2}	737.2	$(\text{V}\cdot\text{s}^2)^{-1}$
δ_{u1}	-0.83	V
δ_{u2}	0.86	V
k_n	13.66	s^{-1}
k_Q	1856	$(\text{N}\cdot\text{m}\cdot\text{s}^2)^{-1}$
k_v	1.102	s^{-1}
k_{Uv}	67.37	m^{-1}
k_w	0.89	--
k_{Tv}	0.01232	$\text{m}(\text{N}\cdot\text{s}^2)^{-1}$
k_U	0.2396	s^{-1}
k_{UU}	1.258	m^{-1}
k_{TU}	4.855×10^{-3}	$\text{m}(\text{N}\cdot\text{s}^2)^{-1}$

Table 4.2: HL & HQ Paramater Values

Parameter	HL Value	HQ Value	Units
c_n^T	1.467×10^{-3}	1.467×10^{-3}	$\text{N}\cdot\text{s}^2$
c_{nv}^T	0.4146	0.3755	$\text{N}\cdot\text{s}^2\cdot\text{m}^{-1}$
c_v^T	0	37.71	$\text{N}\cdot\text{s}^2\cdot\text{m}^{-2}$
c_n^Q	2.804×10^{-6}	2.804×10^{-6}	$\text{N}\cdot\text{m}\cdot\text{s}^2$
c_{nv}^Q	1.296×10^{-11}	9.948×10^{-12}	$\text{N}\cdot\text{s}^2$
c_v^Q	0	9.975×10^{-8}	$\text{N}\cdot\text{s}^2\cdot\text{m}^{-1}$

4.3 State Estimation Methods

An important problem for closed-loop control of the hydrodynamic equations of motion (4.3), (4.4), and (4.5) is gaining knowledge of the axial velocity state v . While this state can be measured directly in experimental settings, it is typically not measurable when considering a full vehicle system [8, 18, 39]. Therefore, estimation methods are required to reconstruct an estimate of v from available measurements [18, 39].

Fossen and Blanke [18] propose a Lyapunov-based nonlinear observer design to reconstruct the unmeasured state v with access to knowledge of the other two states n and U . With $y = U$, and $\tilde{y} = y - \hat{y}$ the observer equations are

$$\dot{\hat{v}} = -k_v \hat{v} - k_{Uv} \hat{v} (|\hat{v}| - k_w \operatorname{sgn}(n)y) + k_{Tv} T(n, \hat{v}) + k_{11} \tilde{y} + |n| k_{12} \tilde{y} \quad (4.16)$$

$$\dot{\hat{U}} = -k_U \hat{U} - k_{UU} \hat{U} |\hat{U}| + k_{TU} T(n, \hat{v}) + k_{21} \tilde{y} + |n| k_{22} \tilde{y}. \quad (4.17)$$

It is important to note that the presence of measurement noise is not considered for this form of observer, so optimality is not guaranteed by this estimation method. It was shown, however, that this observer form guarantees globally exponential convergence to the true values of v and U for the HL system [18, 28]. This is valuable when considering robustness of estimation methods, as other nonlinear estimators like the EKF can struggle with divergence in highly nonlinear systems [26, 27]. Also note that estimation of n is not considered here, so when implementing this observer other estimation methods would be necessary to develop an estimate for this state.

It is of interest in current research to consider practical output feedback strategies for the hydrodynamic system (4.3), (4.4), and (4.5) as well as for higher dimensional full vehicle systems. In particular, optimal estimation in the presence of measurement noise is a vital aspect of modern control design, and would be advantageous if implemented for the full hydrodynamic system while maintaining the robustness of the nonlinear observer in (4.16) and (4.17). With this in mind, a hybrid estimation strategy using both Fossen and Blanke’s nonlinear observer as well as an EKF is proposed for practical implementation of the observer while introducing some considerations for measurement noise in the estimates. This can be accomplished by manipulating the linear gains k_{11} and k_{21} in the observer equations as in an EKF.

According to the derivation of the nonlinear observer, global exponential stability (GES) is maintained as long as the gains satisfy [18, 28]

$$|k_{11}| < \sqrt{2k_v\beta} \tag{4.18}$$

$$k_{21} > \frac{1}{2}\beta - k_U \tag{4.19}$$

for $\beta > 0$. If these gains are calculated from a Kalman gain matrix, they will be optimal for the system in (4.3), (4.4), and (4.5) linearized about \hat{n} , \hat{v} , and \hat{U} . Note that the resulting estimates will be suboptimal due to the nonlinear gains also present in (4.16) and (4.17) but will remain exponentially convergent to the true states. If the Kalman gains fall outside of the acceptable range for convergence, they can be saturated to maintain GES, or remain unaltered to more effectively filter

noise out of the estimates. The restrictions on gain choice for the observer have been shown to be fairly conservative, and relaxing them improved some performance in simulation [18]. Note also that an EKF here can be used to obtain locally optimal estimates of n as well. Fossen and Blanke's nonlinear observer and the EKF hybrid variant will be denoted by the abbreviations NLO and KFNLO respectively in the next chapter when comparing performance.

Lastly, it is of value to consider how to determine the nominal value of the ambient velocity U surrounding an individual thruster when incorporated in a multi-thruster full vehicle system. Consider the simplified assumption that the vector of ambient velocities for all thrusters \mathbf{U} relates to the vehicle state $\boldsymbol{\nu}$ by

$$\mathbf{U} = K_v \boldsymbol{\nu}, \tag{4.20}$$

then it can be shown that given knowledge of the thruster orientation matrix K_t the following is true:

$$K_v = K_t^T. \tag{4.21}$$

Therefore, under this assumption an approximation for the state vector \mathbf{U} will be available if knowledge of $\boldsymbol{\nu}$ is available.

4.4 Feedback Control Strategy

Extensions of the hydrodynamic system (4.3), (4.4), and (4.5) to feedback control strategies are fairly straightforward and amenable to the previously discussed

control strategy (3.12) [18]. Angular velocity n remains the only directly actuated state, as other states are simply compensated for in conventional controller designs [18]. To obtain a setpoint n_d for feedback control, the HL model has been shown to yield the following expression [18]:

$$n_d = \frac{c_{nv}\hat{v} + \operatorname{sgn}(T_d)\sqrt{(c_{nv}\hat{v})^2 + |4c_n^T T_d|}}{2c_n^T}. \quad (4.22)$$

Similarly, for the HQ model the following holds:

$$n_d = \frac{c_{nv}\hat{v} + \operatorname{sgn}(T_d)\sqrt{(c_{nv}\hat{v})^2 + |4c_n^T(c_v^T\hat{v}|\hat{v}| + T_d)|}}{2c_n^T}. \quad (4.23)$$

Therefore, the control law (3.12) can be used in feedback control with axial flow compensation with minimal alteration.

An important change for feedback control of the hydrodynamic system is compensation of axial flow in the feedforward term of (3.12). In particular, knowledge of $Q(n, v)$ is not available, and in fact $Q(\hat{n}, \hat{v})$ must be used instead. This can result in decreased tracking performance if the estimates have not fully converged to the true states yet. In order to compensate for such model perturbations, the control law (3.12) can be augmented with an integral term to ensure steady-state tracking and improve robustness of the control strategy [18, 25, 40]. Additionally, replacing \hat{n} with n_d in the feedforward portion of the control law can ensure better convergence to the setpoint as it removes dependence on estimates that may be inaccurate [18].

The control law (3.12) then becomes

$$u = \gamma^{-1}(\alpha) \tag{4.24}$$

$$\alpha = \dot{n}_d + k_n n_d + k_Q Q(n_d, \hat{v}) - k_P(\hat{n} - n_d) - k_I \sigma \tag{4.25}$$

$$\dot{\sigma} = \hat{n} - n_d. \tag{4.26}$$

Note that this control strategy can be used for both the HL and HQ models.

An extension of the Lyapunov analysis from Chapter 3 yields no further insight for either the single-thruster or full vehicle system as the dynamics for v and U are not stabilized but rather compensated. Experimental and simulated closed-loop performance is discussed in the next chapter using (4.24) as well as the NLO and KFNLO estimators.

Chapter 5: Performance Evaluation of Thrust Control

It is of interest to evaluate the setpoint-tracking performance of the control methods (3.12) and (4.24) with the different models presented in the previous chapters. Many of the dynamic models have been validated experimentally, but have not been fully evaluated in terms of their improvement of feedback control over the simplified model (3.8) [8, 16–18, 39]. In particular, control methods with estimation using the NLO model (4.16) and (4.17) and the HL model for thrust and torque have been tested through simulation only for a single-thruster, forward-moving vehicle [18]. Closed-loop control tests also have not been performed for a HQ model of thrust, therefore it is unclear how much performance benefit is expected when using these models for model-based control design [16, 20].

This chapter aims to thoroughly test and compare output feedback control performance using all the models and estimation methods outlined in previous chapters. Section 5.1 outlines the methods and findings of single-thruster control experiments performed in a flow tank, and section 5.2 seeks to further draw comparisons between control methods based on full vehicle control simulations using a multi-thruster system. Both sections compare tracking control results for all models from previous chapters using the control law (4.24) while also varying the estimation method for

constructing \hat{v} . The choice of model and estimator (if needed) constitute the independent variable for the experiments and simulations, while dependent variables are primarily thrust setpoint tracking for the experiments and vehicle trajectory setpoint tracking for simulations.

5.1 Experimental Performance of Single-Thruster Control

5.1.1 Experimental Methodology

Experimental comparison of thrust tracking control performance of the output feedback method in (4.24) using the observer in (4.16) and (4.17) is an essential next step for improving thruster control design. Multiple scenarios were tested to provide a variety of comparisons and allow strong conclusions to be drawn on the value of model-based control accounting for fluidic effects on thrust. The NLO and KFNLO were both used in output feedback experiments of a single thruster in a flow tank using the control law (4.24) and compared to the performance of the same control scheme with estimates provided by an EKF. Additionally, all three output feedback methods were implemented for both the HL and HQ models of thrust and torque (i.e. using (4.22) or (4.23) to calculate n_d) and an EKF was additionally used to estimate n for the control law (3.12) using the simplified model (3.8). All scenarios were compared to a naïve strategy of an open loop test using a lookup table method of prescribing inputs based on (3.6) and data presented in Fig. 3.6. Additionally, all models and output feedback methods were tested in tracking three different thrust setpoint scenarios: a step, triangle wave, and sine wave of desired thrust T_d .

The feedback control experiments were performed in a Loligo Systems flow tank with a 25×25 cm cross section. The same experimental setup used for system identification of the hydrodynamic models (see Fig. 4.1) including the six-axis load cell and ADV were used to implement control methods and collect data of thrust performance. The ADV was used to provide real-time measurements of ambient fluid velocity to run the observers while the load cell recorded thrust output in each scenario that was run. An Arduino Mega was used to provide voltage input commands to the thruster and obtain sensor measurements from the tachometer and ADV. The control law and observers were implemented in a Matlab program that communicated directly with the Arduino. Each control scenario was run with a 25 Hz sampling frequency for controller and observer iteration. A block diagram of the general output feedback method is depicted in Fig. 5.1

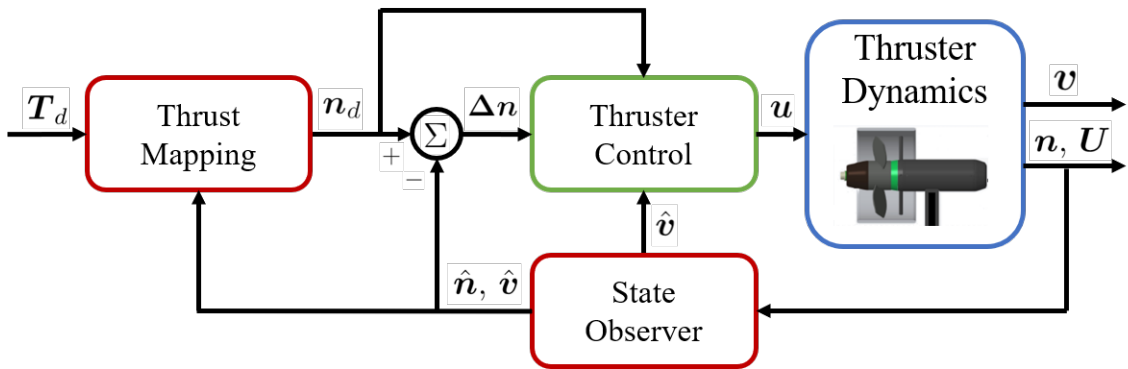


Figure 5.1: Block diagram of the feedback loop used for experimental output feedback tests of the thruster. When using the simplified model for control purposes, inclusion of v and U is omitted from this framework.

5.1.2 Discussion of Results

Fossen and Blanke [18] evaluate the performance of output feedback using the NLO against traditional PI control for a simulated single-thruster system. Findings suggest steady-state errors are greater for the PI control that does not use the NLO for output feedback compared to the NLO-based output feedback controller [18]. However, such a conclusion ignores the fact that all models for thruster dynamics are based on steady-state data of thrust, so any model-based control would achieve low steady-state tracking errors in practice. In truth, the anticipated benefit of hydrodynamic compensation in output feedback of thrust is almost exclusively in the transient behavior of the system. This is the primary focus of evaluating experimental thruster control methods. Thrust overshoot is anticipated for controllers that do not account for fluidic effects on thrust [11, 17, 39].

Results for the step, triangle wave, and sine wave experiments are presented in Figs. 5.2, 5.3, and 5.4 respectively. Qualitatively, it appears all scenarios display similar performance. In fact maximum thrust tracking errors only ever appear to reach 10% of nominal values. To obtain a more quantitative comparison, root-mean-square tracking errors (RMSE) for thrust were calculated for all runs and normalized by the RMSE of the lookup table performance in each tracking scenario. Additionally, the RMSE was only calculated using the corrected data in the plots of Figs. 5.2 and 5.3 in order to exclude data corrupted by load cell ringing.

The RMSE for each scenario are presented in Fig. 5.5 for the step, triangle wave, and sine wave experiments respectively. While results vary between scenarios,

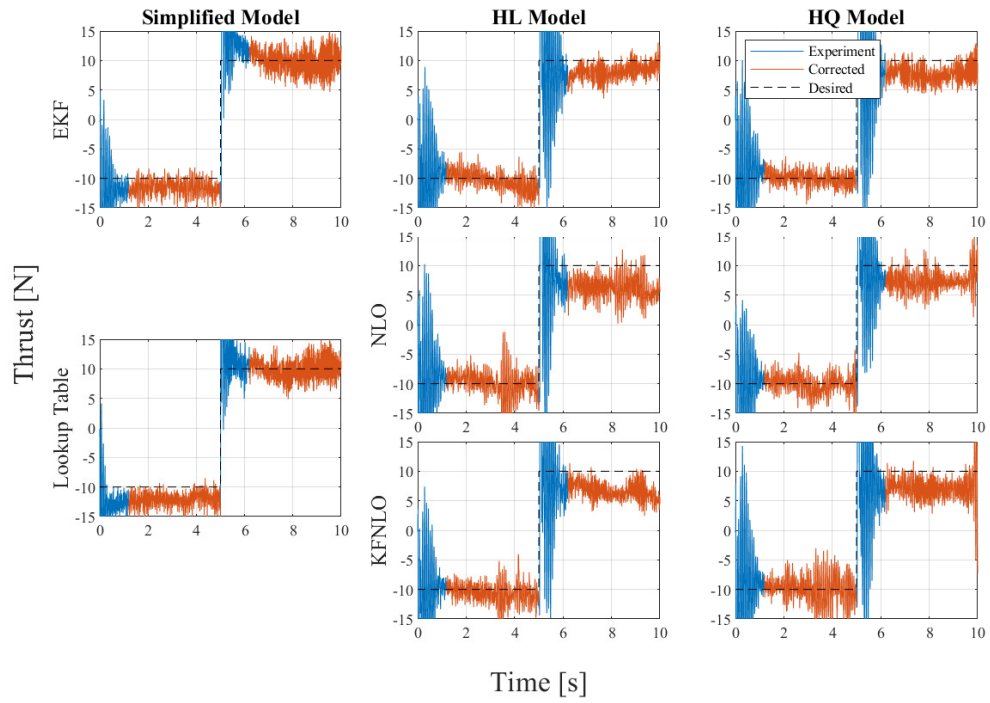


Figure 5.2: Tracking performance of thrust for the step experimental run.

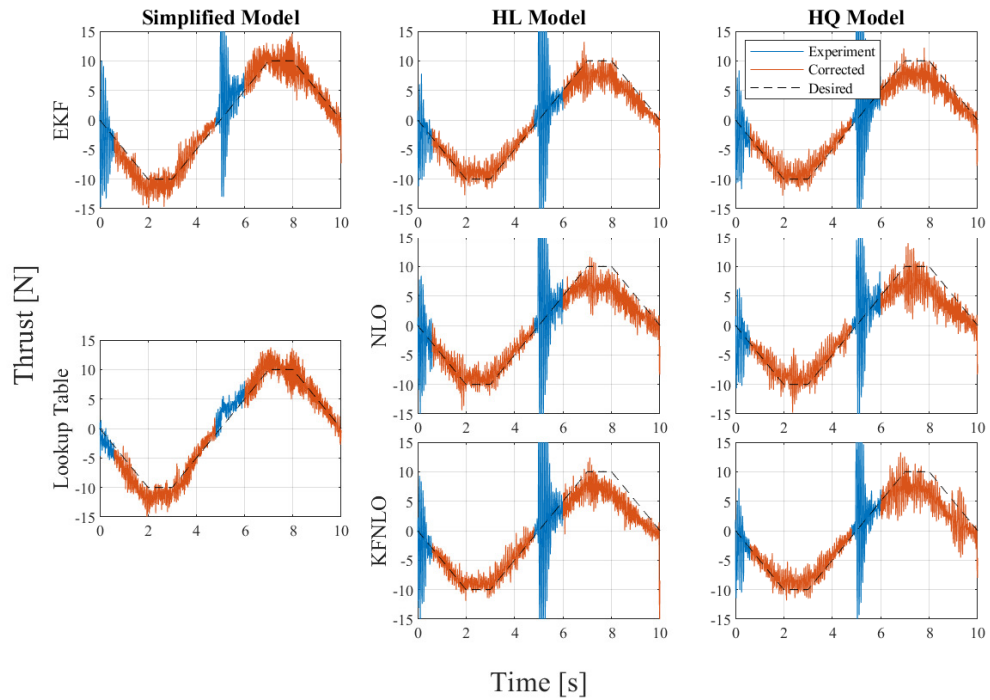


Figure 5.3: Tracking performance of thrust for the triangle wave experimental run.

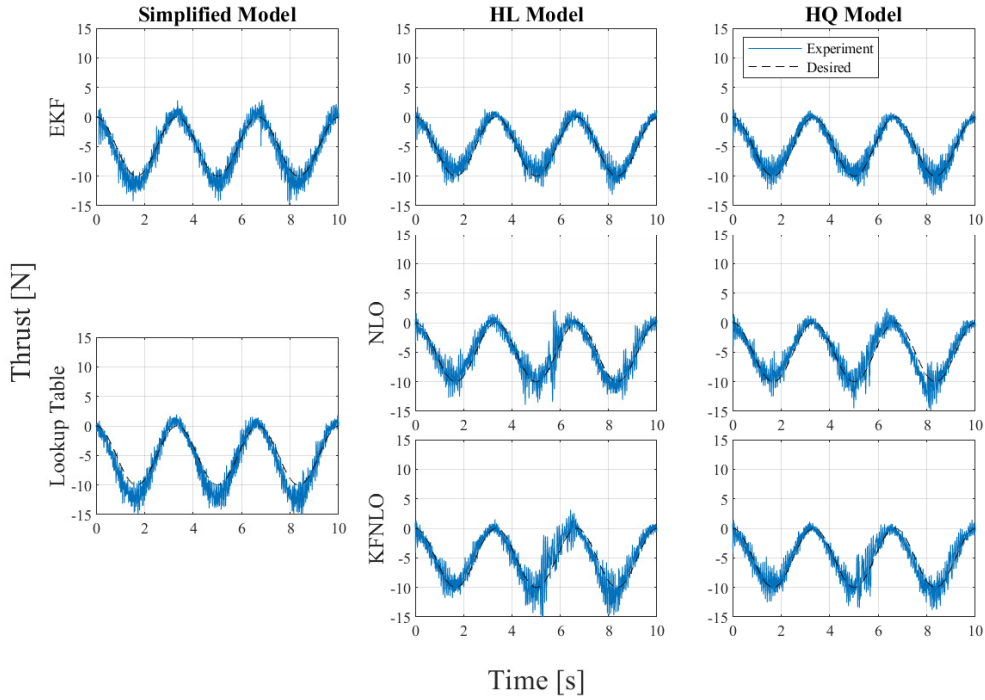


Figure 5.4: Tracking performance of thrust for the sine wave experimental run.

it appears that the EKF-based output feedback methods perform best at minimizing thrust tracking error compared to the lookup table method. Additionally, smaller performance gains seem apparent when using the HQ model compared to the HL model, but all performance improvements are considerably modest compared to the lookup table as all scenarios perform very similarly.

Fig. 5.6 displays the tracking and estimation performance of the output feedback of angular velocity n for the sine wave scenario. All scenarios track setpoints well, suggesting that the control law (4.24) is overall effective for tracking n_d , and any performance deficiencies in tracking T_d would be due to model choice and/or estimator choice.

To compare estimator performance, Fig. 5.7 presents the time history of velocity estimates \hat{v} and \hat{U} for sine wave scenario as well. Note that noise in the

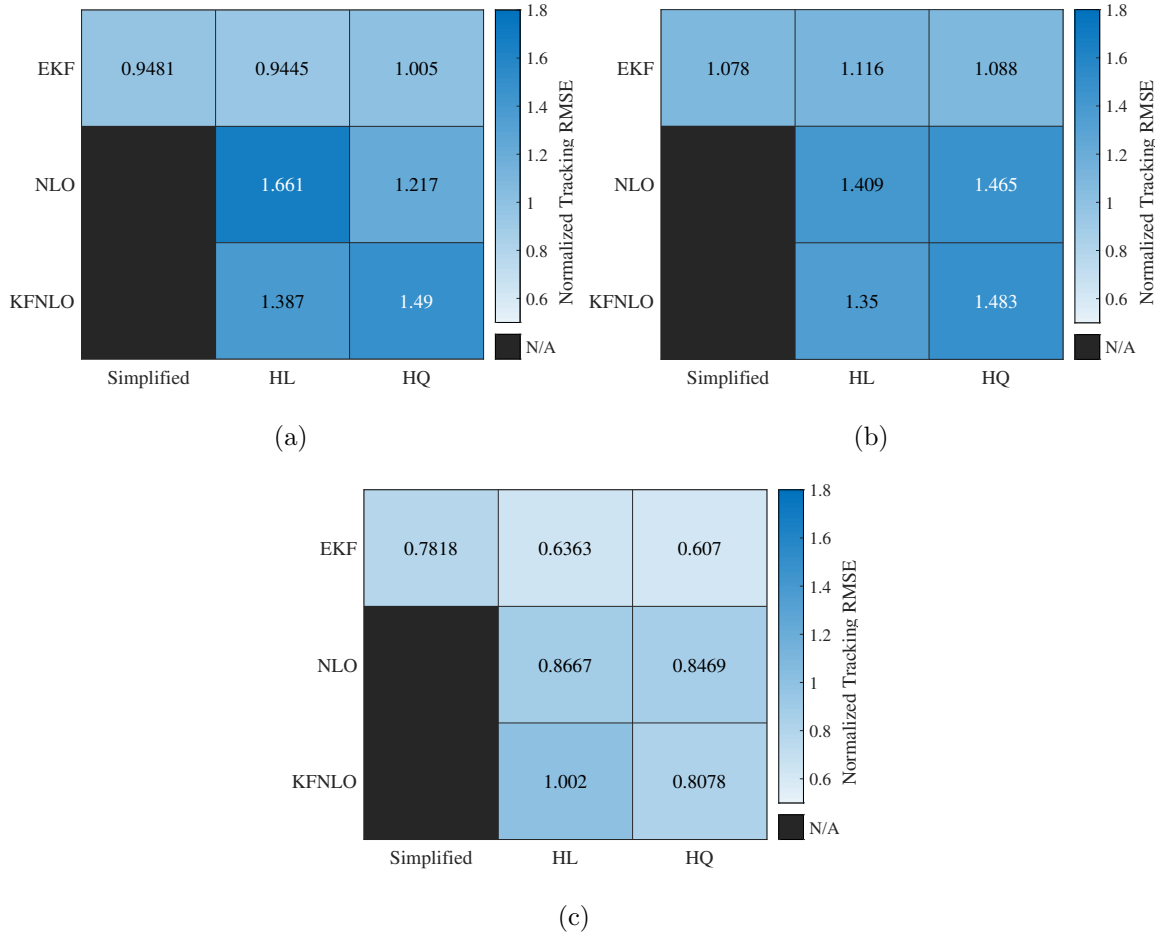


Figure 5.5: Thrust Tracking RMSE normalized by the RMSE of the lookup table method for all control strategies in the test cases for (a) a step, (b) a triangle wave, and (c) a sine wave.

ADV measurements tends to occur intermittently, which is attributed to turbulence created by the thruster itself. The EKF tends to resist these spikes in all scenarios while the NLO and KFNLO fail to do so. While this property of the EKF proves beneficial in these experiments, and could explain the lower performance of the NLO and KFNLO in thrust tracking, it also highlights the fact that the EKF can diverge from the true state if unmodeled perturbations are too great. In contrast, the NLO and KFNLO would guarantee global convergence to the true values of v and U . Lastly, it should be noted that no tracking or estimation improvements are

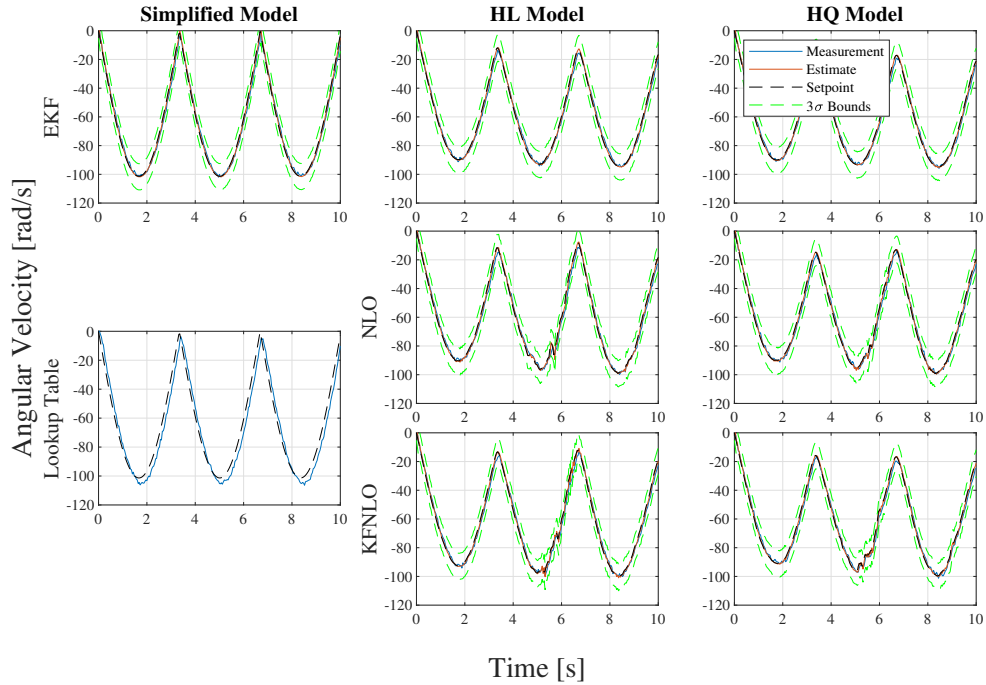


Figure 5.6: Tracking and estimation performance of angular velocity for the sine wave experimental run.

observed for the KFNLO over the NLO.

5.2 Simulated Performance of Full Vehicle Control

Simulations of full vehicle dynamics with simplified thruster models have been performed in previous work [37, 41]. However, multi-thruster systems have not been simulated with hydrodynamic considerations, nor have output feedback control methods been evaluated in such simulations. Therefore additional insight on how output feedback methods compare can be obtained through such simulations.

Full vehicle simulations were performed in two scenarios. First, in section 5.2.1, an underwater vehicle with actuator dynamics behaving according to (3.8) was simulated to compare the setpoint-tracking performance of a vehicle using the dead-zone-

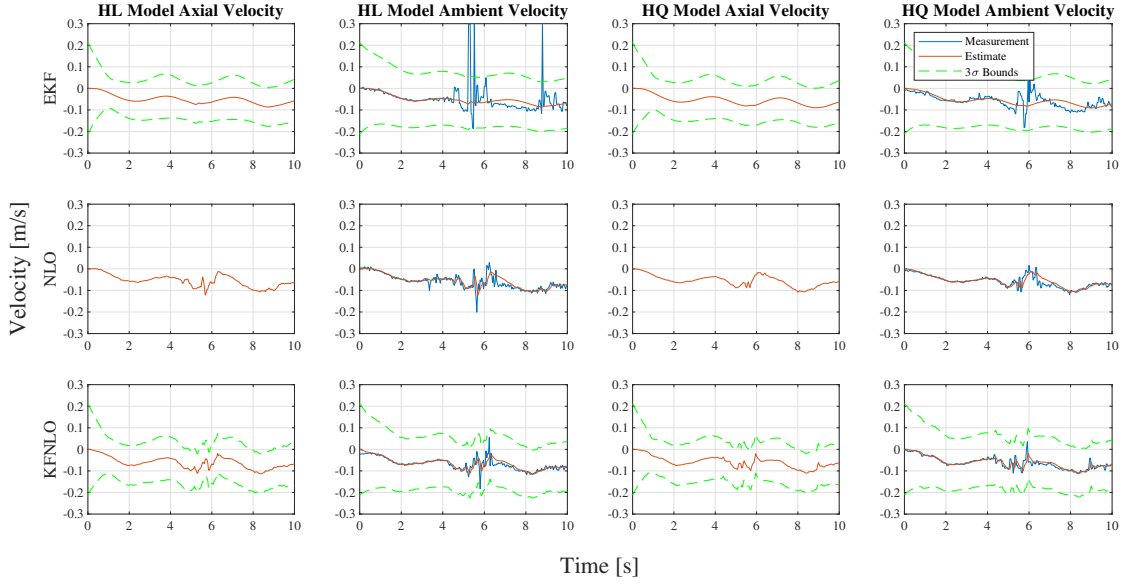


Figure 5.7: Estimation performance of axial and ambient velocity for the sine wave experimental run.

compensating control law (3.12) to one using the open loop lookup table method. Second, in section 5.2.2, all output feedback methods with all models are simulated for a vehicle behaving according to the HQ model to compare performance between model-based controllers using the simplified model against ones using more detailed models. In all simulations, the full vehicle dynamics (2.1) and (2.2) were used with the outer loop thrust control law (2.22) defining thrust setpoints for inner loop control of the thruster dynamics. A block diagram of the full vehicle control scheme is displayed in Fig. 5.8

5.2.1 Simulations with Simple Thruster Model

Simulations of the system (3.24) were performed with the dead-zone-compensating controller (3.12) and compared to a lookup table method of actuator dynamics compensation. Tracking performance of the control scheme compares favorably to the

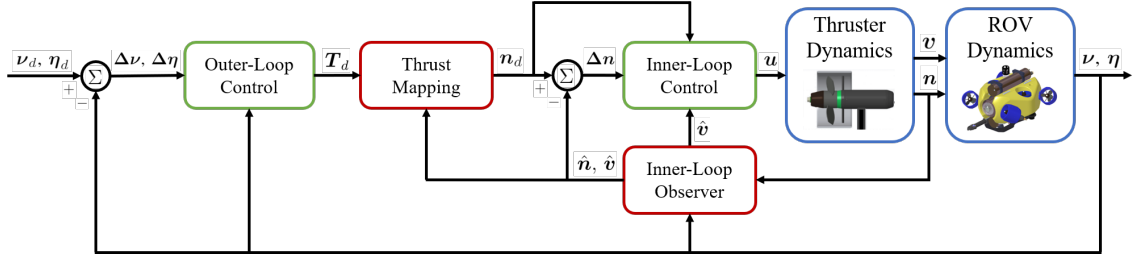


Figure 5.8: Block diagram of the feedback loop used for simulated output feedback tests of the ROV. When using the simplified model for control purposes, inclusion of v is omitted from this framework.

lookup table. Due to the fact that the lookup table method does not account for actuator dynamics, and therefore assumes rapid convergence to steady-state propeller speed, deficiencies appear in the setpoint-tracking performance of the overall control scheme.

Fig. 5.9 indicates superior performance of the dead-zone-compensating controller over the lookup-table method. The tracking task involves varying setpoints in forward velocity, pitch rate, and pitch. Parameter values used in simulation of the thruster dynamics are reported in Table 3.1.

To further compare performance of the control methods, the tracking RMSE was calculated for each degree of freedom over the course of the simulation time period and normalized by the average value of the setpoint of each respective degree of freedom. Normalized RMSE results are presented in Fig. 5.10. The dead-zone-compensating controller displays comparable tracking performance in linear velocities when compared to the lookup-table method, but significant improvement comes in tracking attitude and angular velocity setpoints, with tracking errors being reduced by as much as 50%. Divergence from the reference setpoint displayed in the performance of the lookup-table controller is attributed to the trade-off of

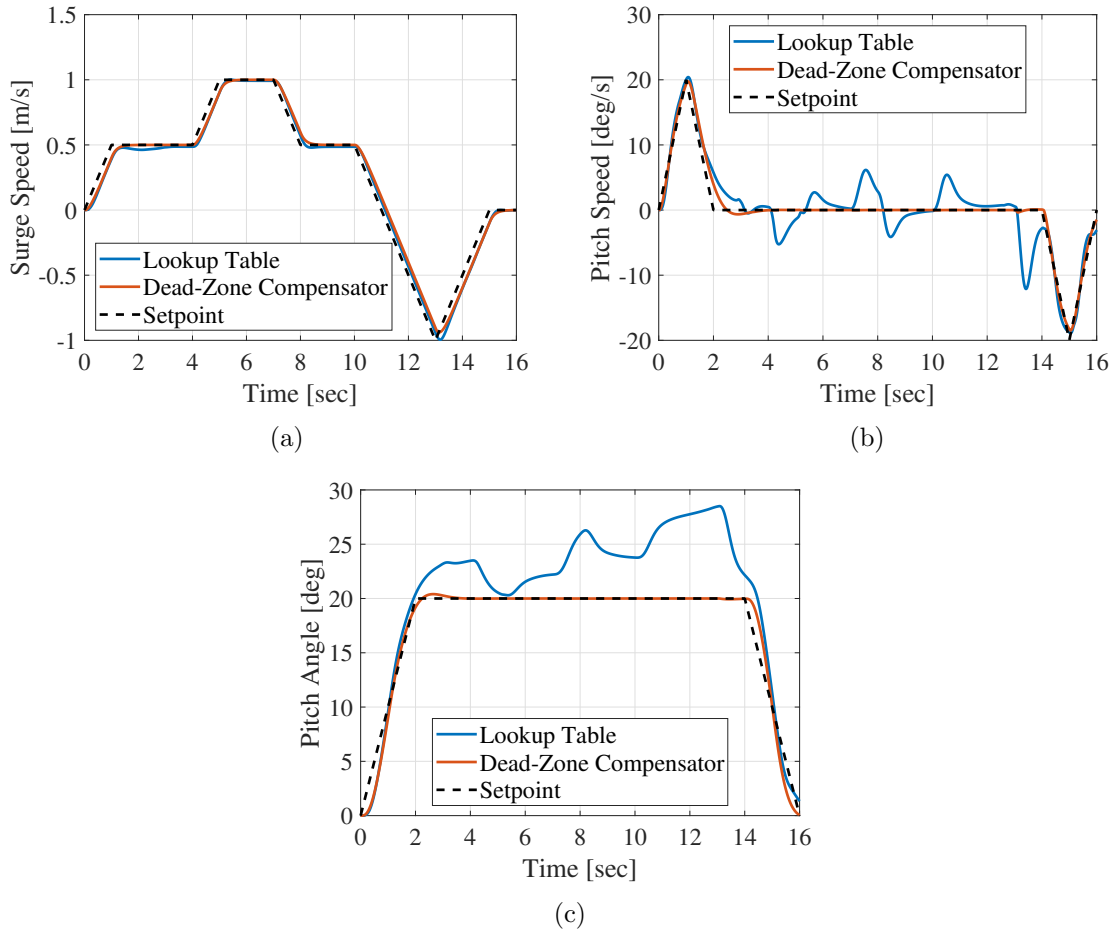


Figure 5.9: Setpoint tracking performance comparison between the proposed dead-zone-compensating controller and lookup-table-based control for (a) linear forward velocity, (b) angular pitch velocity, and (c) pitch angle.

tracking forward velocity with the other states, as multiple setpoints were processed simultaneously.

5.2.2 Simulations with Hydrodynamic Thruster Model

Similar simulation tasks to those in Fig. 5.9 were used to compare output feedback performance when simulating the motion of an underwater vehicle with a HQ model of actuator dynamics. Surge speed, pitch rate, and pitch setpoints were tracked in eight simulations encompassing all estimation methods and all models

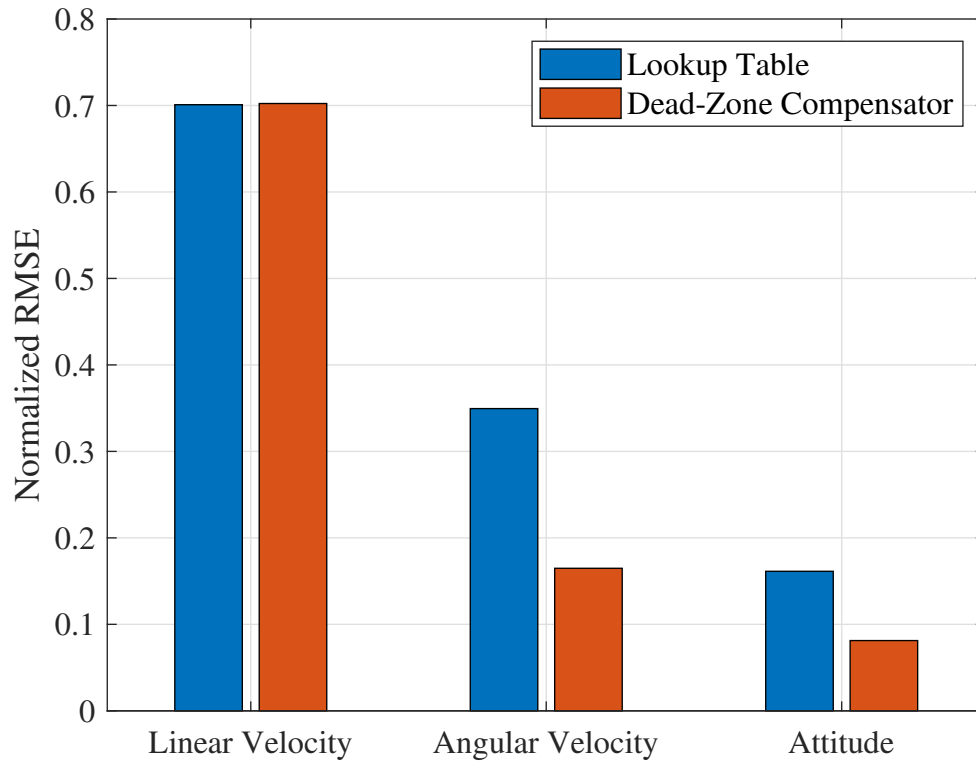


Figure 5.10: Tracking errors for each degree of freedom involved in setpoint tracking.

for control design. Additionally simulated Gaussian noise was included in artificial measurements to allow further evaluation of estimation methods. All scenarios were tested with the same measurement noise.

Results presented in Fig. 5.11 suggest tracking control improvements can be made by using some sort of fluid dynamics compensation in thruster control. Parameter values used in simulation of the thruster dynamics are reported in Table 3.1 for the simplified and lookup table methods and in Table 4.1 for the other output feedback methods as well as the ground-truth simulations.

Comparing normalized tracking RMSE again in Fig. 5.12 for the new simulations allows further remarks to be made. First, it appears that use of the EKF in

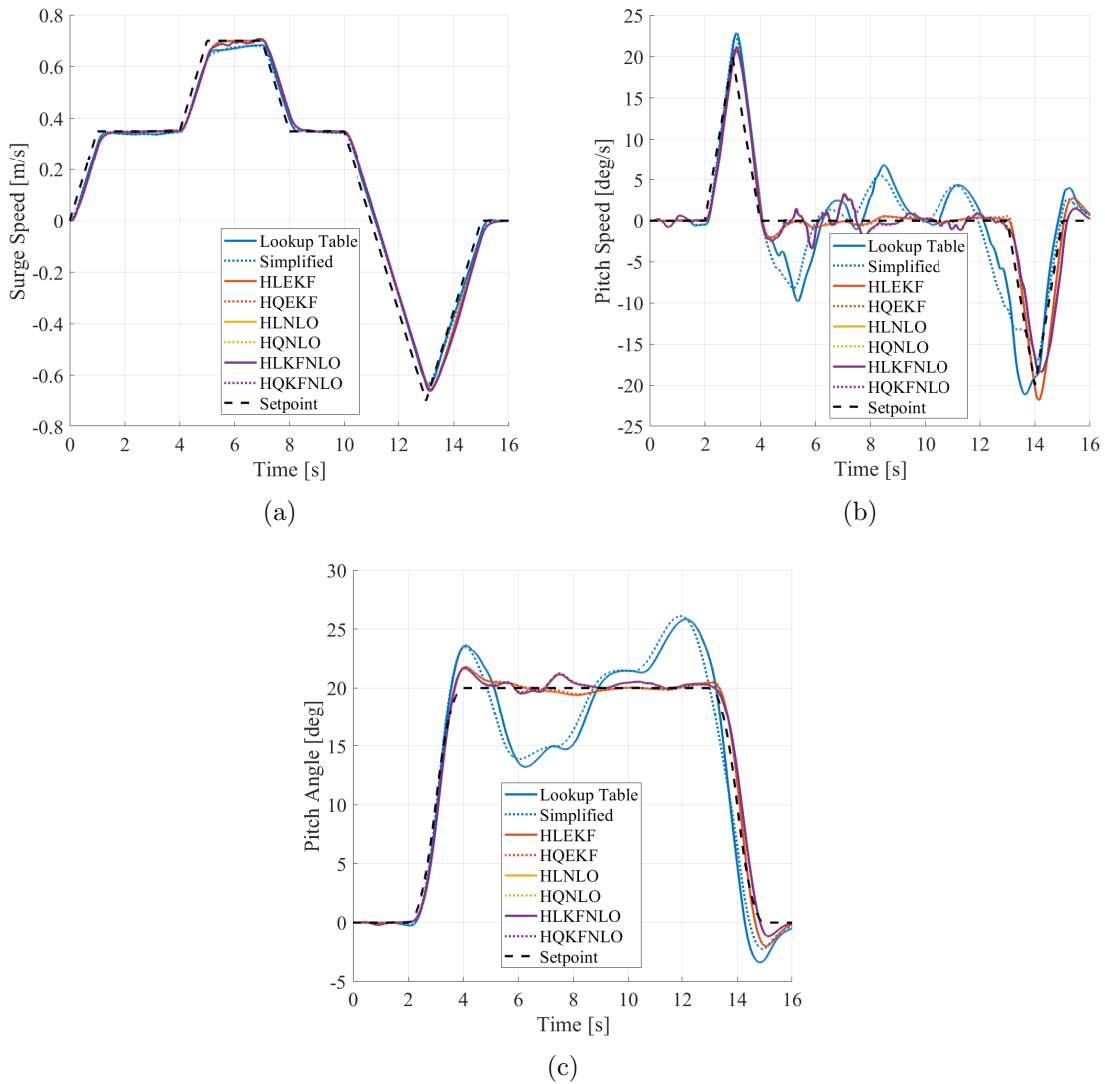


Figure 5.11: Setpoint tracking performance comparison between all the proposed control strategies for (a) linear forward velocity, (b) angular pitch velocity, and (c) pitch angle.

output feedback promises better performance than any iteration of the NLO. This is likely due to the local optimality of the EKF, which even appears better than the KFNLO. In fact, there appears to be no discernible benefit to the KFNLO over the NLO presumably because the exponential convergence property of the observer dominates over any filtering that could be performed. Second, linear velocity appears to be well tracked by all cases, so performance benefits will probably only

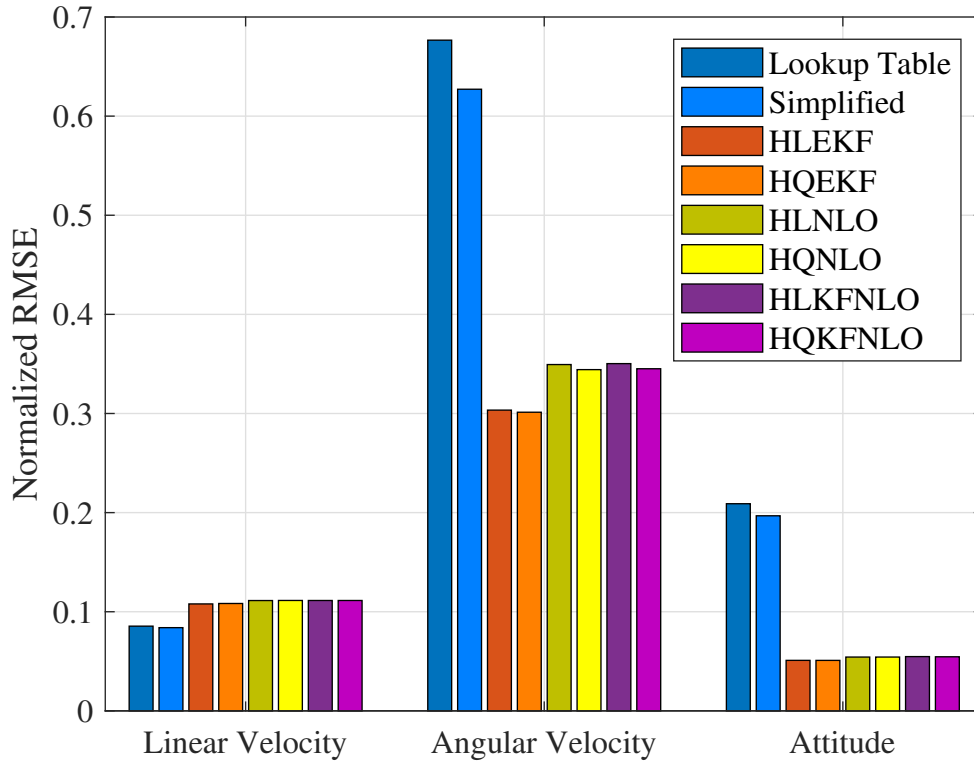


Figure 5.12: Tracking errors for each degree of freedom involved in setpoint tracking.

be noticeable in attitude tracking for a physical implementation. Lastly, although some improvement over the simplified and lookup table scenarios is observed, the HQ model-based control only slightly outperforms the control using the approximated HL model. Therefore the tradeoff between model complexity and performance improvement appears less justifiable.

Estimation of v is an additional metric available in simulation to compare the value of the NLO to other estimators. Time-series estimation errors of v for a single thruster are presented in Fig. 5.13 for all hydrodynamic estimation scenarios, and the estimation RMSE normalized by the average true value for all thrusters in each scenario are displayed in Fig. 5.14. The EKF again displays superior performance

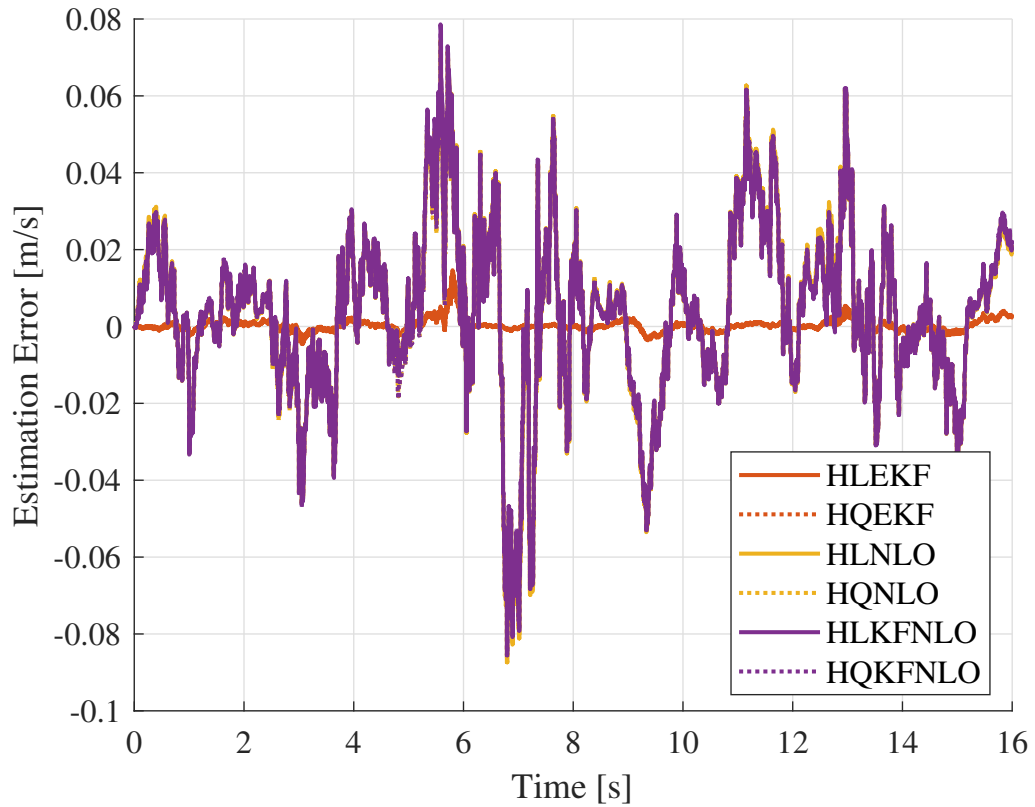


Figure 5.13: Estimation errors of v for an individual thruster in the previous simulations.

over other scenarios, and divergence does not appear an issue in simulation. Although the NLO and KFNLO are valuable for their robustness against divergence, it appears that the EKF is sufficient for obtaining accurate estimates of v .

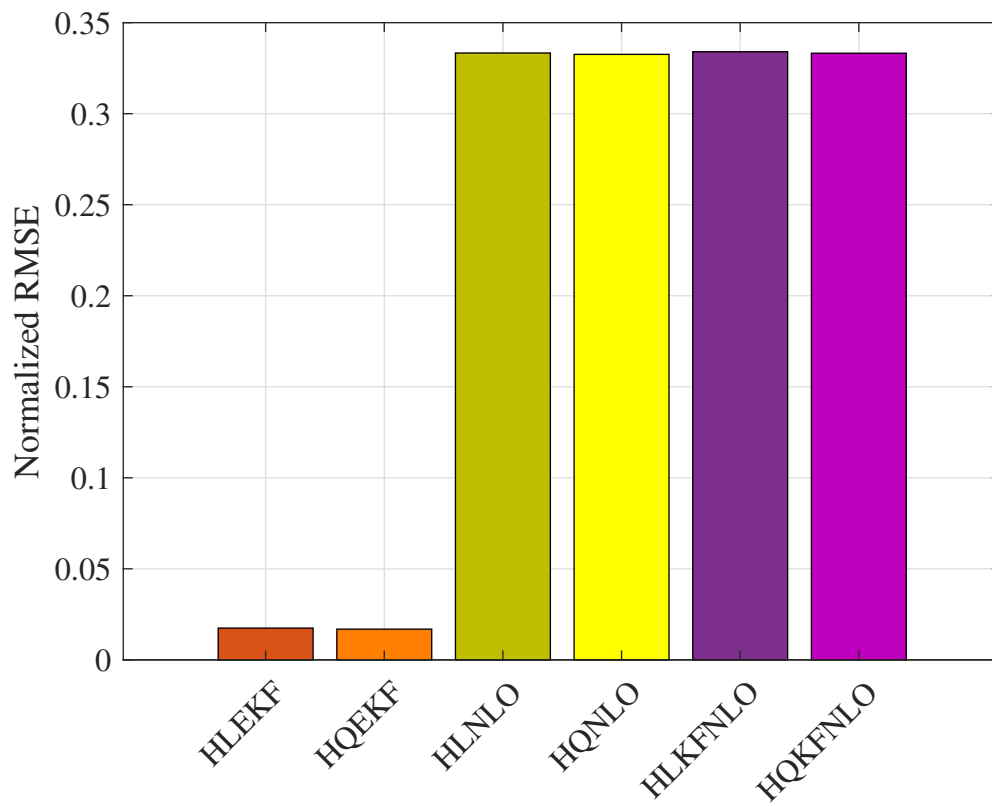


Figure 5.14: Normalized estimation RMSE of v for each estimator run in simulation.

Chapter 6: Conclusion

6.1 Summary of Contributions

The modeling and control of thruster dynamics remains an important aspect of underwater vehicle control. Compensation for these dynamics in simulations of full vehicle, multi-thruster implementations suggests notable improvements in tracking control performance even while experiments suggest minimal improvement for an individual thruster.

In this work, a novel method of system identification for thruster dynamics using a six-axis load cell is presented, and thrust and torque data collected with it are used to characterize a variety of models. The models exhibit good agreement with collected data in cases when lower-order models were characterized as well as in the cases of higher-order model characterization. Nonlinear control principles are used to derive control laws that exponentially stabilize the dynamics in the presence of strong nonlinearities like input dead zones as well as the nonlinear effects of reaction torque. Additionally, these control strategies are extended to implementations that compensate for the effects of fluid dynamics on the thrust output of the system. To enable such implementations, a variety of estimation methods to reconstruct an unmeasured fluid velocity state are presented. Practical integration

of these estimation methods with previously discussed control designs is outlined to motivate experimental and simulated evaluation of all the models and output feedback methods.

The discussed control and estimation strategies offer a variety of combinations for closed-loop output feedback control of a thruster. The availability of such options warrants comparisons to evaluate the benefits of model-based control that accounts for fluidic effects over simpler model-based strategies, as well as comparisons between estimation methods. A nonlinear observer derived by Fossen and Blanke [18] was compared experimentally to other estimation methods with noise considerations in output feedback tests with a thruster in a flow tank. These experiments constituted the first time such a method of fluid compensation was implemented on a physical testbed.

Simulations of tracking control for a multi-thruster ROV were also used to evaluate performance benefits from incorporating this observer compared to others. Both experimentally and in simulations, simplified and hydrodynamic model-based controllers were used with either the NLO, KFNLO, or EKF to draw a wide range of comparisons. Experimental results suggest nominally similar thrust tracking performance among all models used for output feedback control design, while the EKF allows for more optimal estimates of fluid velocity to be obtained compared to the other estimators. In simulation, control methods that compensate for thruster dynamics offer improved tracking performance for a full vehicle over ones that do not account for some higher-order terms. Additionally, the EKF again allows for improved performance over the other estimation methods, despite the possibility

of divergence. However, all control methods can accomplish simulation tasks adequately, suggesting only marginal performance improvements should be expected when attempting to implement the control methods experimentally on a full ROV.

6.2 Suggestions for Ongoing and Future Work

Extensions of this work could seek to include additional models, improved testbeds, and further experimental results to provide further insight into the thruster systems that have been analyzed thus far. An iteration on the six-axis load cell design would benefit from including structural resonance damping so that reactions to sudden transient changes in thrust will not cause such intense ringing that would complicate data collection. Transient behavior of the thruster models would be better characterized with such an improvement. Additionally, transient thrust tracking in closed-loop experiments would be more verifiable with such a setup.

Additional thruster models that assume a steady definition of axial fluid velocity as a linear combination of propeller angular velocity and ambient fluid velocity would be useful comparisons to current experiments and simulations [16]. In such a model, nonlinear estimation considerations would be less necessary due to assumed knowledge of the unmeasured state v based on the other states. Additionally, Kim and Chung [16] derive models for thrust generation of thrusters oriented away from the direction of ambient flow. While these models require the identification of more parameters, their extension for ROV thruster control would be a natural extension of the methods outlined in this work, and would serve for another valuable comparison

case in experiments and simulations.

Lastly, experimental tests with a full vehicle were not addressed and would be a necessary next step in evaluating all the outlined models and output feedback methods that have been discussed. Experimental control performance of an ROV may very well yield different conclusions from simulation results, and additional thruster models could also be compared on such a testbed for more conclusive results.

Bibliography

- [1] M. Ludvigsen, F. Søreide, K. Aasly, S. Ellefmo, M. Zylstra, and M. Pardey. ROV based drilling for deep sea mining exploration. In *OCEANS Aberdeen*, pages 1–6, June 2017.
- [2] R. Nian, B. He, J. Yu, Z. Bao, and Y. Wang. ROV-based underwater vision system for intelligent fish ethology research. *International Journal of Advanced Robotic Systems*, 10(9):326, 2013.
- [3] S. Negahdaripour and P. Firoozfam. An ROV stereovision system for ship-hull inspection. *IEEE Journal of Oceanic Engineering*, 31(3):551–564, July 2006.
- [4] S. M. Nornes, M. Ludvigsen, Ø. Ødegard, and A. J. Sørensen. Underwater photogrammetric mapping of an intact standing steel wreck with ROV. *IFAC-PapersOnLine*, 48(2):206 – 211, 2015.
- [5] R. D. Christ and R. L. Wernli. *The ROV Manual: A User Guide for Remotely Operated Vehicles*. Elsevier, Waltham, MA, USA, second edition, 2014.
- [6] S. C. Martin and L. L. Whitcomb. Preliminary experiments in fully actuated model based control with six degree-of-freedom coupled dynamical plant models for underwater vehicles. In *IEEE International Conference on Robotics and Automation*, pages 4621–4628, May 2013.
- [7] S. C. Martin and L. L. Whitcomb. Nonlinear model-based tracking control of underwater vehicles with three degree-of-freedom fully coupled dynamical plant models: Theory and experimental evaluation. *IEEE Transactions on Control Systems Technology*, 26(2):404–414, March 2018.
- [8] W. M. Bessa, M. S. Dutra, and E. Kreuzer. Dynamic positioning of underwater robotic vehicles with thruster dynamics compensation. *International Journal of Advanced Robotic Systems*, 10(9):325, 2013.

- [9] L. G. Garca-Valdovinos, T. Salgado-Jimnez, M. Bandala-Snchez, L. Nava-Balazar, R. Hernndez-Alvarado, and J. A. Cruz-Ledesma. Modelling, design and robust control of a remotely operated underwater vehicle. *International Journal of Advanced Robotic Systems*, 11(1):1, 2014.
- [10] P.-M. Lee, B.-H. Jeon, Se.-W. Hong, Y.-K. Lim, C.-M. Lee, J.-W. Park, and C.-M. Lee. System design of an ROV with manipulators and adaptive control of it. In *Proceedings of the International Symposium on Underwater Technology*, pages 431–436, May 2000.
- [11] A. J. Healey, S. M. Rock, S. Cody, D. Miles, and J. P. Brown. Toward an improved understanding of thruster dynamics for underwater vehicles. *IEEE Journal of Oceanic Engineering*, 20:354–361, Oct 1995.
- [12] M. Blanke, K.-P. Lindegaard, and T. I. Fossen. Dynamic model for thrust generation of marine propellers. *IFAC Proceedings Volumes*, 33(21):353 – 358, 2000.
- [13] R. Bachmayer, L. L. Whitcomb, and M. A. Grosenbaugh. An accurate four-quadrant nonlinear dynamical model for marine thrusters: theory and experimental validation. *IEEE Journal of Oceanic Engineering*, 25(1):146–159, Jan 2000.
- [14] L. Pivano, T. A. Johansen, and Ø. N. Smogeli. A four-quadrant thrust estimation scheme for marine propellers: Theory and experiments. *IEEE Transactions on Control Systems Technology*, 17(1):215–226, Jan 2009.
- [15] D. R. Yoerger, J. G. Cooke, and J.-J. E. Slotine. The influence of thruster dynamics on underwater vehicle behavior and their incorporation into control system design. *IEEE Journal of Oceanic Engineering*, 15(3):167–178, July 1990.
- [16] J. Kim and W. K. Chung. Accurate and practical thruster modeling for underwater vehicles. *Ocean Engineering*, 33(5):566 – 586, 2006.
- [17] L. L. Whitcomb and D. R. Yoerger. Development, comparison, and preliminary experimental validation of nonlinear dynamic thruster models. *IEEE Journal of Oceanic Engineering*, 24(4):481–494, Oct 1999.
- [18] T. I. Fossen and M. Blanke. Nonlinear output feedback control of underwater vehicle propellers using feedback form estimated axial flow velocity. *IEEE Journal of Oceanic Engineering*, 25(2):241–255, April 2000.
- [19] J. Boehm, E. Berkenpas, C. Shepard, and D. A. Paley. Feedback-linearizing control for velocity and attitude tracking of an ROVs with thruster dynamics containing input dead zones. In *2019 Annual American Control Conference (ACC)*, July 2019.

- [20] J. Kim. Thruster modeling and controller design for unmanned underwater vehicles (UUVs). In Alexander V. Inzartsev, editor, *Underwater Vehicles*, chapter 13. IntechOpen, Rijeka, 2009.
- [21] X. Wu, X. Wu, and X. Luo. Adaptive control of nonlinearly parameterized system with unknown dead-zone input. In *8th World Congress on Intelligent Control and Automation*, pages 3811–3815, July 2010.
- [22] N. F. Jasim and I. F. Jasim. Robust control design for spacecraft attitude systems with unknown dead zone. In *IEEE International Conference on Control System, Computing and Engineering*, pages 375–380, Nov 2011.
- [23] J. Boehm, E. Berkenpas, B. Henning, M. Rodriguez, C. Shepard, and A. Turchik. Characterization, modeling, and simulation of an ROV thruster using a six degree-of-freedom load cell. In *OCEANS 2018 MTS/IEEE Charleston*, pages 1–7, Oct 2018.
- [24] L. Pivano, T. A. Johansen, Ø. N. Smogeli, and T. I. Fossen. Nonlinear thrust controller for marine propellers in four-quadrant operations. In *2007 American Control Conference*, pages 900–905, July 2007.
- [25] H. K. Khalil. *Nonlinear Systems*. Pearson Education. Prentice Hall, 2002.
- [26] J. L. Crassidis and J. L. Junkins. *Optimal Estimation of Dynamic Systems*. Chapman & Hall/CRC Applied Mathematics & Nonlinear Science. CRC Press, 2004.
- [27] S. Särkkä. *Bayesian Filtering and Smoothing*. Bayesian Filtering and Smoothing. Cambridge University Press, 2013.
- [28] J. Jouffroy and J. Lottin. A remark on "nonlinear output feedback control of underwater vehicle propellers using feedback from estimated axial flow velocity". *IEEE Journal of Oceanic Engineering*, 27(4):873–875, Oct 2002.
- [29] P. Giguere, C. Prahacs, and G. Dudek. Characterization and modeling of rotational responses for an oscillating foil underwater robot. In *2006 IEEE/RSJ International Conference on Intelligent Robots and Systems*, pages 3000–3005, Oct 2006.
- [30] K. Muljowidodo, S. Adi N., N. Prayogo, and A. Budiyo. Design and testing of underwater thruster for shrimp ro-v-itb. *Indian Journal of Marine Sciences*, 38(3):338–345, Sep 2009.
- [31] Q. Liang, D. Zhang, Y. Wang, and Y. Ge. Design and analysis of a novel six-component f/t sensor based on cpm for passive compliant assembly. *Measurement Science Review*, 13(5):253–264, 2013.

- [32] A. Ghosal. Six component force-torque sensors using gough-stewart platform manipulators. *Annals of the Indian National Academy of Engineering*, 8:79–88, Jan 2011.
- [33] R. Ranganath, P. S. Nair, T. S. Mruthyunjaya, and A. Ghosal. Studies on a stewart platform based force torque sensor in a near-singular configuration. In *Proceedings of the 11th World Congress in Mechanism and Machine Science*, 2003.
- [34] Y. Zhao, T. Zhao, R. Wen, and H. Wang. Performance analysis and optimization of sizable 6-axis force sensor based on stewart platform. In *2007 International Conference on Mechatronics and Automation*, pages 2189–2193, Aug 2007.
- [35] T. I. Fossen. *Handbook of Marine Craft Hydrodynamics and Motion Control*. Wiley, 2011.
- [36] H. D. Nguyen, S. Malalagama, and D. Ranmuthugala. Design, modelling and simulation of a remotely operated vehicle–Part 1. *Journal of Computer Science and Cybernetics*, 29(4):299–312, 2013.
- [37] Ø. N. Smogeli, A. J. Sørensen, and T. I. Fossen. Design of a hybrid power/torque thruster controller with loss estimation. *IFAC Proceedings Volumes*, 37(10):409 – 414, 2004. IFAC Conference on Computer Applications in Marine Systems - CAMS 2004, Ancona, Italy, 7-9 July 2004.
- [38] A. Saunders and M. Nahon. The effect of forward vehicle velocity on through-body AUV tunnel thruster performance. In *OCEANS '02 MTS/IEEE*, volume 1, pages 250–259 vol.1, Oct 2002.
- [39] L. L. Whitcomb and D. R. Yoerger. Preliminary experiments in model-based thruster control for underwater vehicle positioning. *IEEE Journal of Oceanic Engineering*, 24(4):495–506, Oct 1999.
- [40] A. Lora, T. I. Fossen, and A. Teel. Ugas and ules of nonautonomous systems: Applications to integral control of ships and manipulators. In *1999 European Control Conference (ECC)*, pages 1517–1522, Aug 1999.
- [41] D. Di Vito, E. Cataldi, P. Di Lillo, and G. Antonelli. Vehicle adaptive control for underwater intervention including thrusters dynamics. In *2018 IEEE Conference on Control Technology and Applications (CCTA)*, pages 646–651, Aug 2018.